Supporting Information

for

Impact of Pressure and Temperature on the Broadband Dielectric Response of the HKUST-1 Metal-Organic Framework

Arun S. Babal,[a] Lorenzo Donà,[b] Matthew R. Ryder,[c] Kirill Titov,[a] Abhijeet K. Chaudhari,[a] Zhixin Zeng,[a] Chris S. Kelley,[d] Mark D. Frogley,[d] Gianfelice Cinque,[d] Bartolomeo Civalleri,[b] and Jin-Chong Tan[a,]*

[a]Multifunctional Materials and Composites (MMC) Laboratory, Department of Engineering Science, University of Oxford, Parks Road, Oxford, OX1 3PJ, United Kingdom

[b]Department of Chemistry, NIS and INSTM Reference Centre, University of Turin, *via* Pietro Giuria 7, 10125 Torino, Italy

[c]Neutron Scattering Division, Oak Ridge National Laboratory, Oak Ridge, Tennessee 37831, United States

[d]Diamond Light Source, Harwell Campus, Chilton, Oxford, OX11 0DE, United Kingdom

[*]E-mail: jin-chong.tan@eng.ox.ac.uk

Table of Contents

1. Material and characterization

1.1 Material

The HKUST-1 (copper benzene-1,3,5-tricarboxylate) MOF material also known as Basolite C300 was purchased from Sigma Aldrich and used without further purification.

1.2 Pellet preparation

The HKUST-1 pellets with a diameter of 13-mm were prepared under different mechanical loads (0.5, 1, 2, 3, 5, 7 and 10 tons force) using a hydraulic press (Specac 15 tons capacity). The pellet mass was kept constant at 150 mg. The pellets were designated as Nt, where N is the applied mechanical load during pelleting. The calculated nominal density was the ratio of individual pellet mass to the pellet volume.

1.3 Optical microscopy and surface profilometry

Alicona profilometer was used to measure the surface texture such as roughness of the MOF pellet. The surface topography was characterized by infinite focus microscopy technique (Alicona Infinite Focus 3D profilometer) using the 20× optics on the profilometer.

1.4 Fourier-transform infrared (FTIR) spectroscopy

The FTIR spectra of the pellets were characterized in the mid-IR region at 0.5 cm^{-1} spectral resolution by employing the Nicolet-iS10 FTIR spectrometer equipped with an attenuated total reflection (ATR) accessory.

1.5 Thermogravimetric analyses (TGA)

The thermal stability of the HKUST-1 specimens was measured using the TGA-Q50 (TA Instruments) equipped with an induction heater (max temperature 1000 °C) and platinum sample holder under an N_2 inert atmosphere. The samples were heated at a rate of 10 °C/min from 40 to 500 °C.

1.6 X-ray diffraction (XRD)

The XRD patterns of HKUST-1 powder and pellets were measured using the Rigaku Miniflex bench-top X-ray diffractometer. The data were collected from the Bragg diffraction angle of $2\theta = 2°$ to $30°$, at a scan rate of $1°$/min with a step size of $0.05°$.

2. Experimental setup and analysis of dielectric and reflectivity data

2.1 Using the LCR meter to measure Hz-MHz range

The dielectric response of different pressure pellets was measured using the Hioki-IM3536 LCR meter in the frequency range of 4 Hz to 1.5 MHz, see Figure S1(a). The measurements were based on the principle of a parallel plate capacitor. The two opposing surfaces of each pellet sample coming into contact with the electrodes were coated with a thin layer of silver conducting paint (RS). The parallel plate setup was placed in a vacuum oven with a 50-L chamber, and calibrated (at both open and closed circuit) beforehand in order to eliminate any parasitic impedance and admittance. Before pellet measurements, each sample was first evacuated in the vacuum (10^{-3} bar) for 16 hours and thereafter temperature dependent measurements were carried out with a step increase of 10 °C under the same vacuum environment. The real (ε') and imaginary (ε'') parts of the dielectric constant as a function of frequency (ω) was calculated from the following equations:

$$\varepsilon'(\omega) = \frac{C(\omega)d}{\varepsilon_0 A}$$

$$\varepsilon''(\omega) = \varepsilon'(\omega) \tan \delta$$

where C is the capacitance, d is the distance between the pair of parallel plate electrodes, A is area of the electrode, ε_0 is vacuum permittivity and $\tan \delta$ is the loss tangent.

2.2 Using synchrotron infrared (IR) specular reflectance spectroscopy to measure the far- (THz), mid- and near-IR frequencies

The IR reflectivity spectra of pellets prepared using compression varied from 0.5 to 10 tons were carried out at Beamline B22 MIRIAM in the Diamond Light Source (Harwell, UK), see Figure S1(b). We employed the Bruker Vertex 80V FTIR interferometer equipped with the Pike Technologies VeeMAX II variable angle specular reflectance accessory to measure the specular reflectance spectra under vacuum conditions at room temperature

(21 °C), in the frequency range of 1.5 THz to 150 THz. The specular reflection spectra were collected at an angle of 30° from the normal axis of the pellet surface at 2 cm^{-1} resolution and 512 scans per spectral scan. The 6-μm thick Mylar broadband multi-layer coated beam splitter was used to perform the measurement in far-IR, whereas KBr beam splitter was used for the mid-IR region. The background spectra were collected before each far and mid-IR measurements.

The Kramers-Kronig Transform (KKT) [1] is based on the causality principle that shows the dependency of the real and imaginary part of complex quantities i.e. dielectric constant ($\tilde{\varepsilon}(\omega) = \varepsilon'(\omega) + i\varepsilon''(\omega)$), refractive index ($\tilde{n}(\omega) = n(\omega) + i\kappa(\omega)$) and logarithm of the amplitude-reflectivity on each other. The built-in KKT routine in the Bruker OPUS software only takes piecewise information from the reflectance spectra resulted into the negative values for the imaginary part of refractive index and dielectric constant. The mid- and far-IR reflectivity spectra were smoothly joined together using the MATLAB code to get a continuous reflectance spectra as described in ref. [2].

The phase change (ϕ) at an arbitrary wavenumber (ω_a) was calculated using the Kramers-Kronig relation:

$$\phi(\omega_a) = \frac{2\omega_a}{\pi} \int_0^\infty \frac{\log\left(\sqrt{R(\omega)}\right)}{\omega^2 - \omega_a^2} d\omega$$

The real $n(\omega)$ and imaginary $\kappa(\omega)$ parts of the complex refractive index are given by [3]:

$$n(\omega) = \frac{1 - R(\omega)}{1 + R(\omega) - 2\sqrt{R}\cos(\phi(\omega))}$$

$$\kappa(\omega) = \frac{-2\sqrt{R}\sin(\phi(\omega))}{1 + R(\omega) - 2\sqrt{R}\cos(\phi(\omega))}$$

The relation between complex dielectric constant $\tilde{\varepsilon}(\omega)$ and refractive index $\tilde{n}(\omega)$ can thus be obtained as:

$$\tilde{\varepsilon}(\omega) = \tilde{n}(\omega)^2$$

$$\varepsilon'(\omega) = n(\omega)^2 - \kappa(\omega)^2$$

$$\varepsilon''(\omega) = 2n(\omega)\kappa(\omega)$$
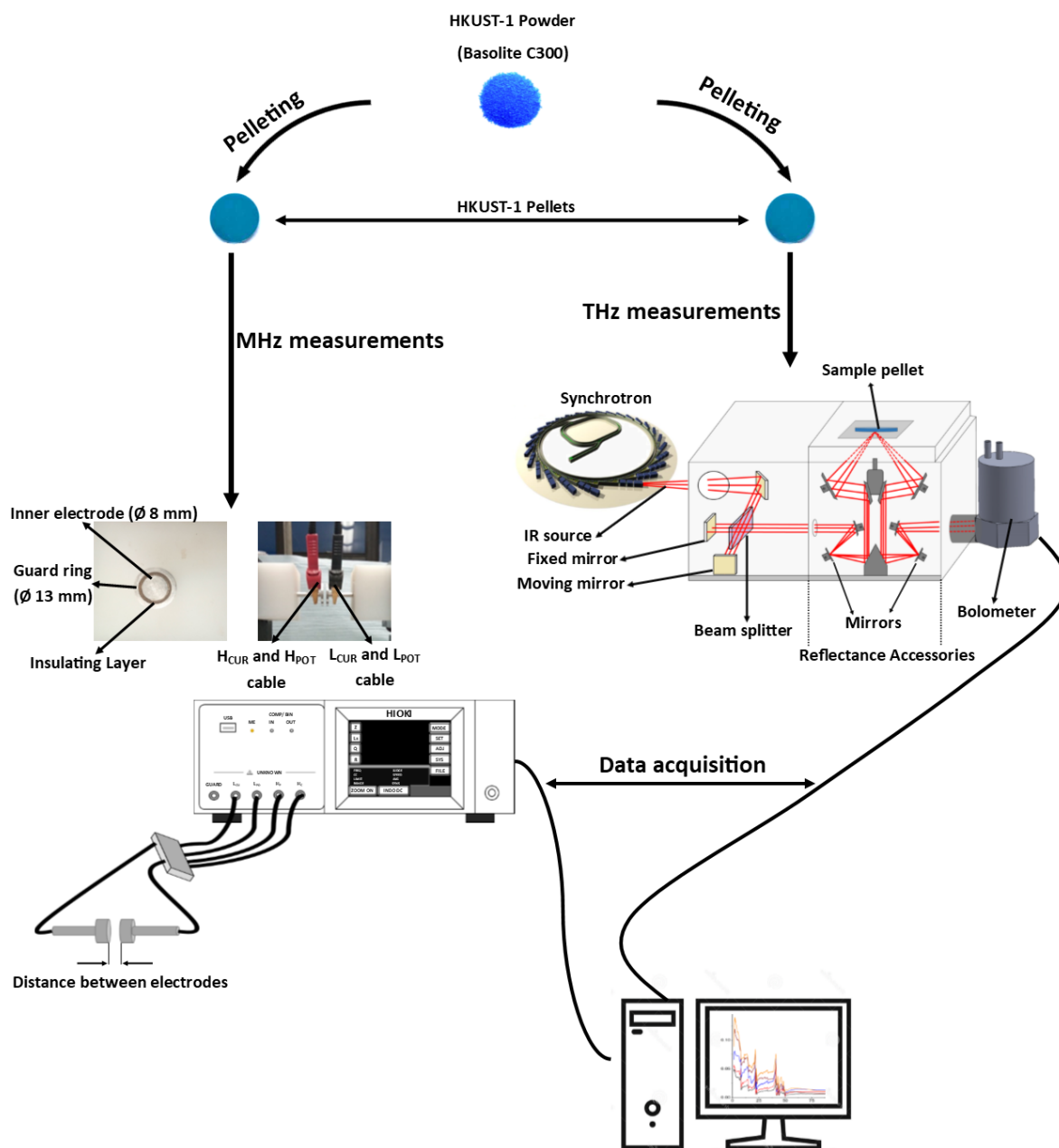
Figure S1: Experimental setups used to conduct the broadband dielectric measurements on the HKUST-1 MOF pellets.

3. Pellets topographic characterization

(a)

(b)

0.5t

RMS=454 nm

12 μm

(c)

(d)

1t

RMS=250.7 nm

12 μm

(e)

(f)

2t

RMS=105.9 nm

12 μm

(g)

(h)

3t

RMS=65.6 nm

12 μm

(i) (j)

5t
RMS=70.5 nm

12 μm

(k) (l)

7t
RMS=75.6 nm

12 μm

(m) (n)

10t
RMS=71.6 nm

12 μm

(o)
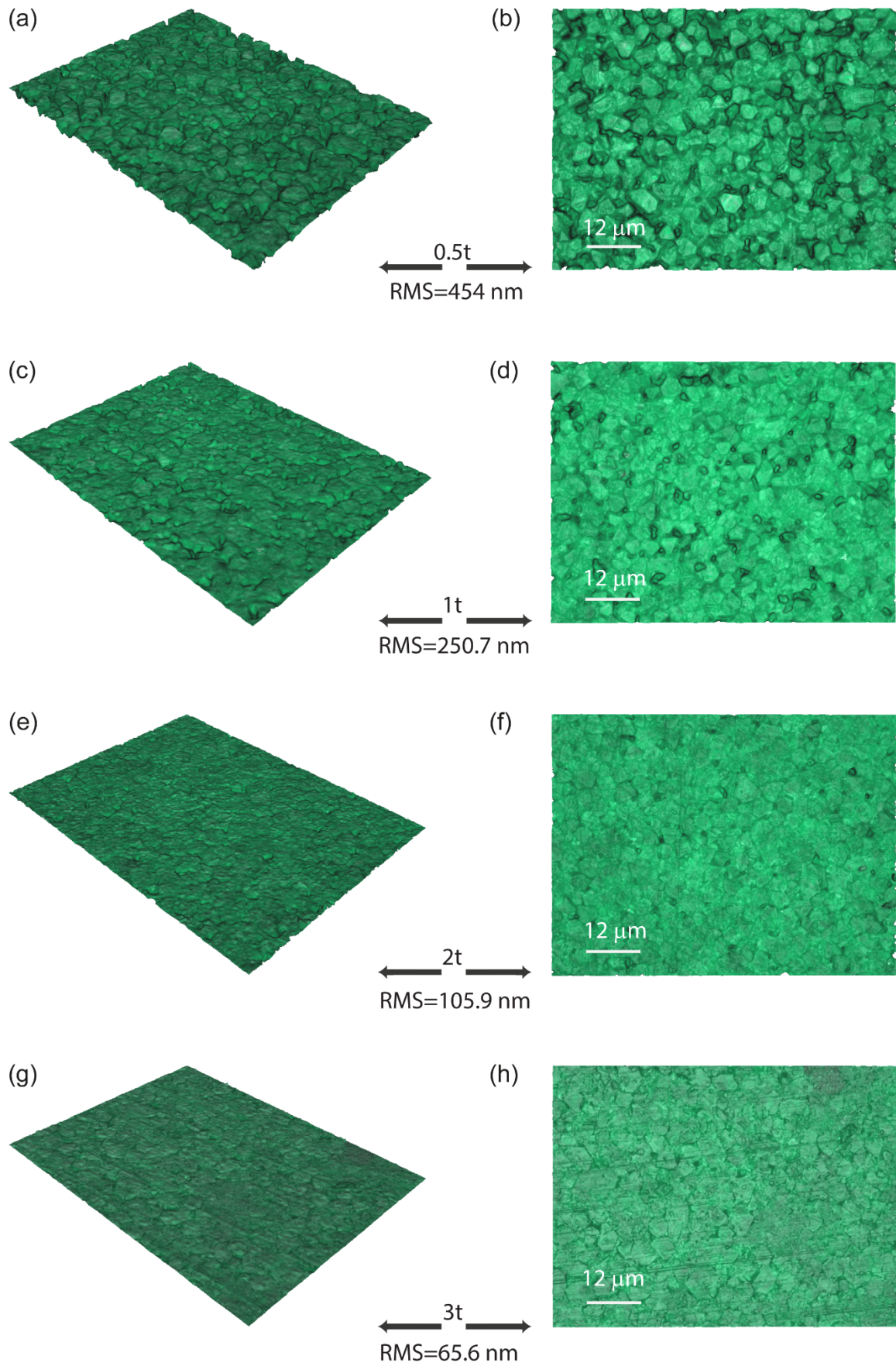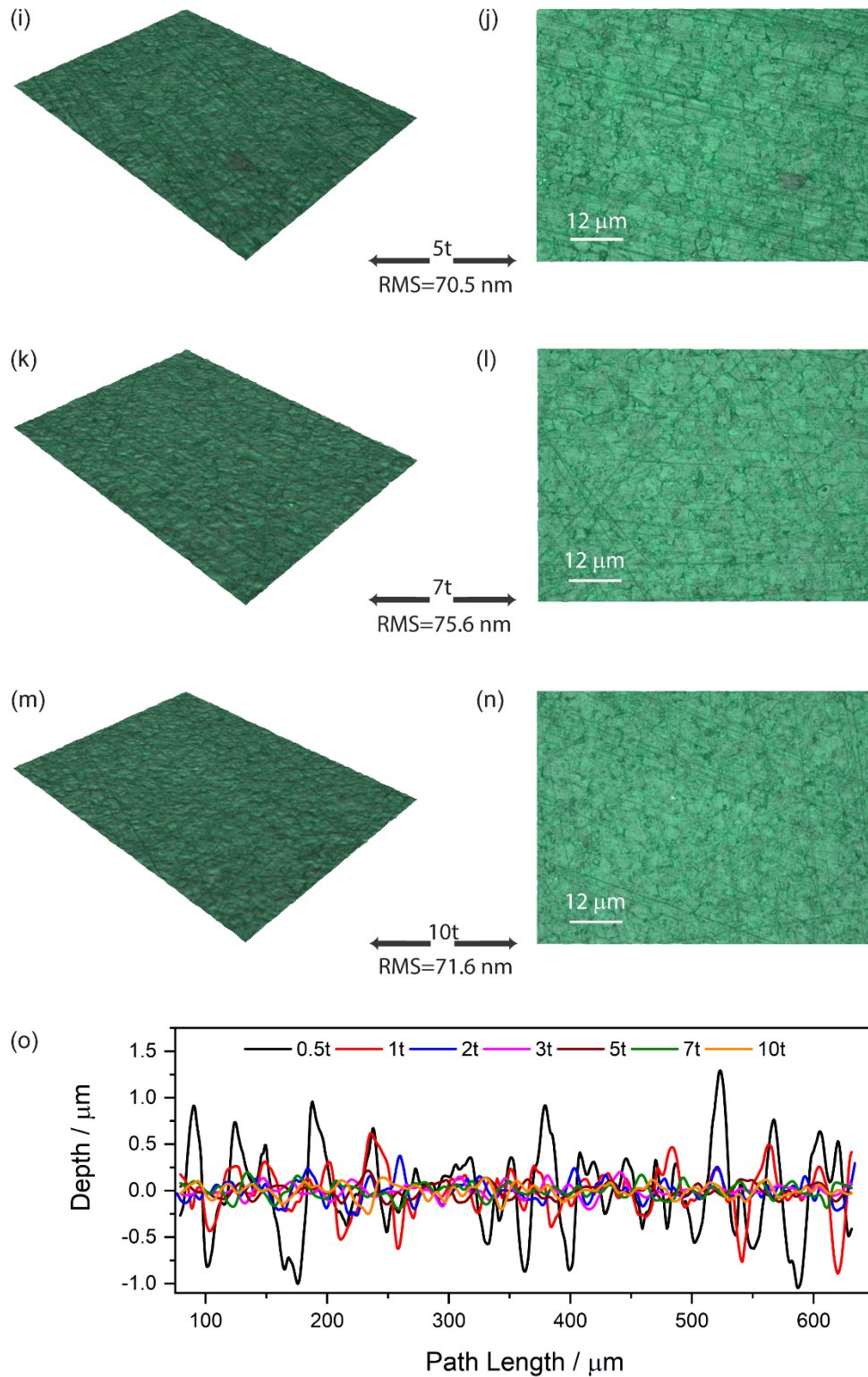
Figure S2: Pellet surface topography characterized using the Alicona Infinite Focus profilometer at 20× optical magnification: (a)-(b) 0.5 ton, (c)-(d) 1 ton, (e)-(f) 2 ton, (g)-(h) 3 ton, (i)-(j) 5 ton, (k)-(l) 7 ton, (m)-(n) 10 ton and (o) Pellet roughness profile (the width of profile line is 80 μm), respectively. RMS represents the root mean squared roughness value of the surface profile.

4. Effect of nominal pressure on FWHM of the XRD reflections

(a)
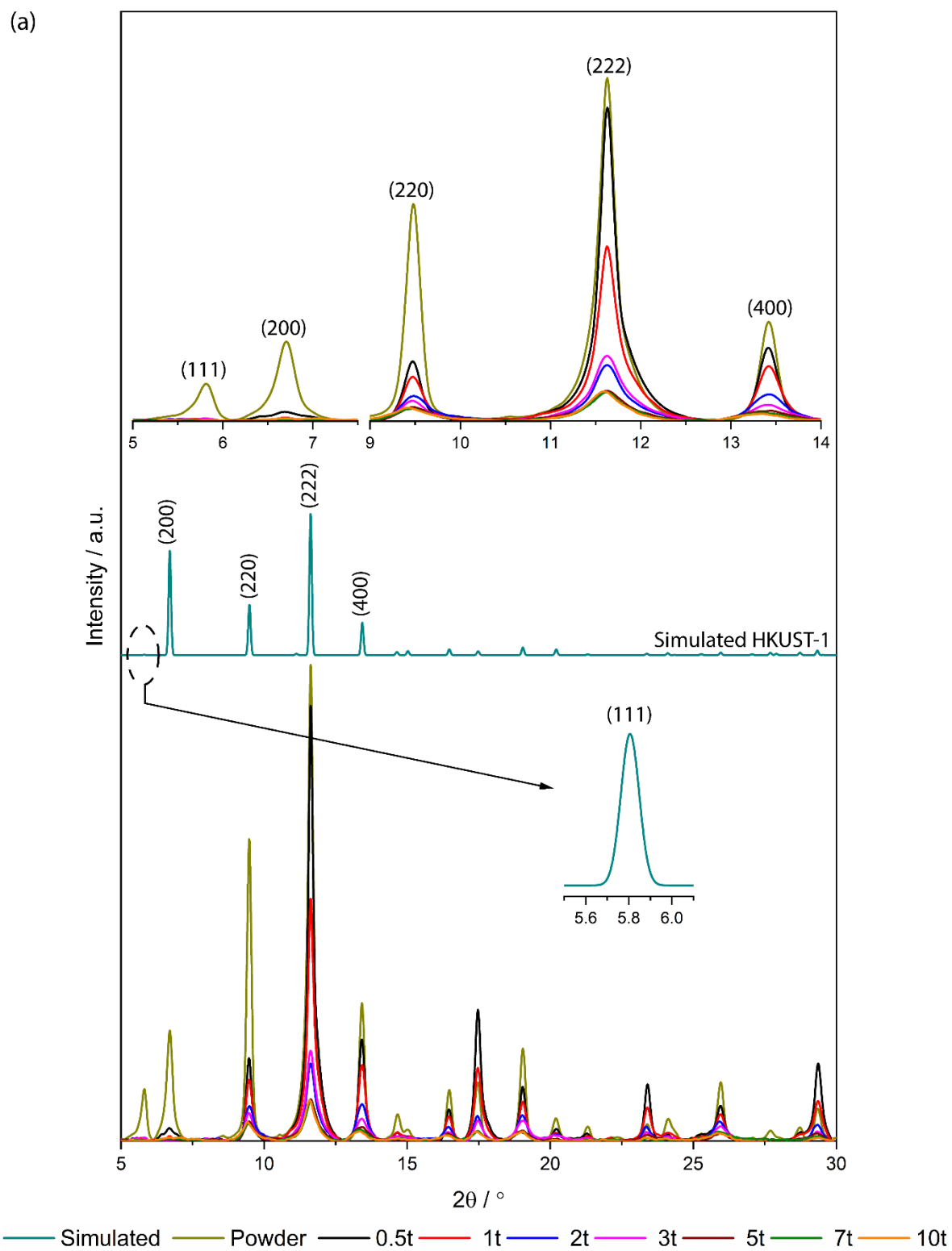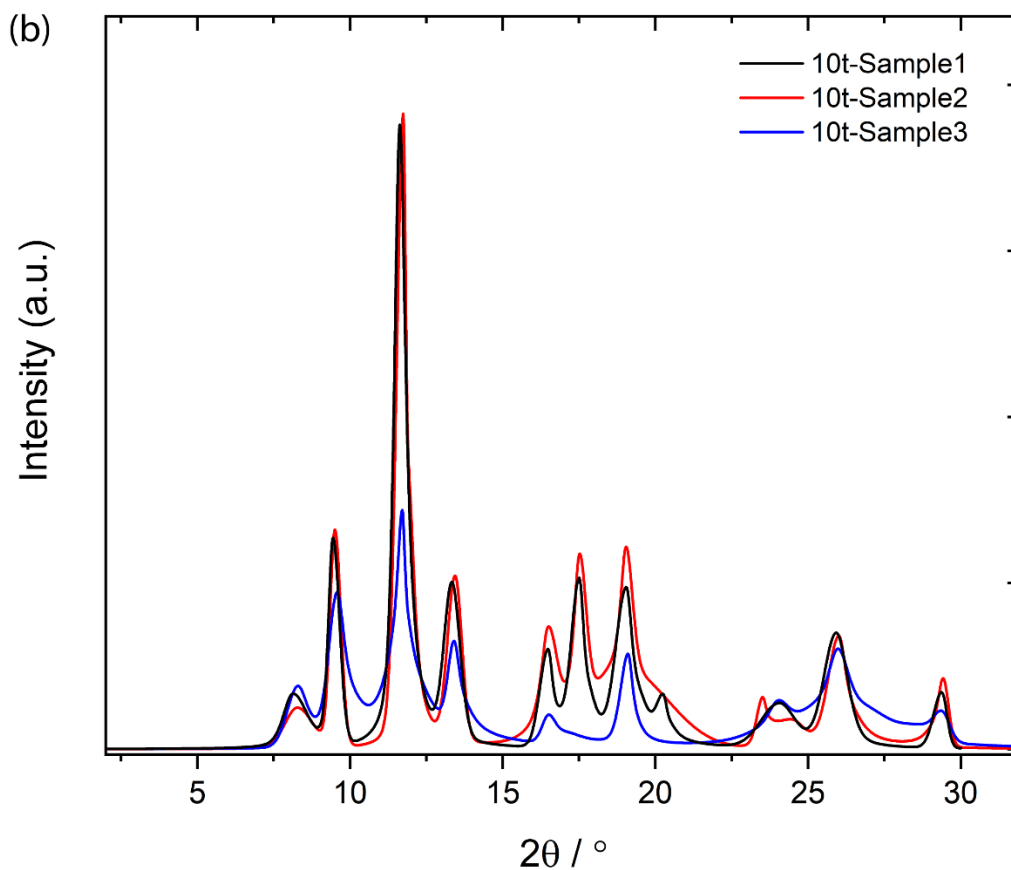
Figure S3: (a) Non-normalized XRD patterns of HKUST-1 samples in absolute intensities. Inset: magnified view of the main characteristic peaks. (b) XRD plot of three different 10t pellets to confirm that amorphization is irreversible. A new 10t pellet (~750 MPa) was prepared to check the repeatability in the XRD spectra. This pellet was then ground into powder and then left for 5 days to recover from the stress. The prepared pellet from this ground powder shows further decline in crystallinity compared to the other 10t pellets. (10t-Sample1 = Previous 10t pellet spectra, 10t-Sample2 = 10t pellet spectra prepared to check repeatability and 10t-Sample3 = 10t pellet prepared from the ground powder of 10t-Sample2 pellet)
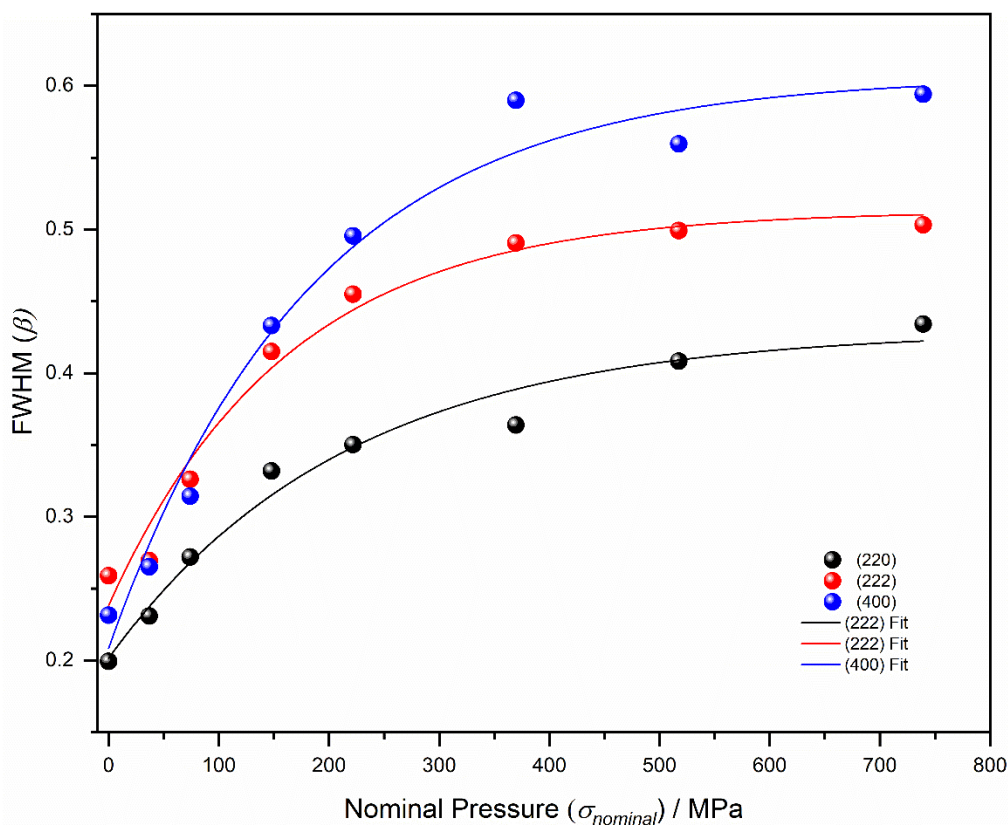
Figure S4: FWHM plot of HKUST-1 MOFs XRD peaks as a function of applied pressure. In this plot effect of pressure on various characteristic planes i.e. (220), (222) and (400) was investigated using the full width at half maximum (FWHM). The curves are following a similar pattern as the nominal density plot indicates that high compression loading is resulting in MOF framework amorphization.

Table S1: FWHM values of XRD planes for different pressure pellets.

Designation	Pressure (MPa)	Characteristics planes of HKUST-1		
		(220)	(222)	(400)
Powder	0	0.20	0.26	0.23
0.5t	36.96	0.23	0.27	0.27
1t	73.92	0.27	0.33	0.31
2t	147.84	0.33	0.42	0.43
3t	221.76	0.35	0.45	0.50
5t	369.60	0.36	0.49	0.59
7t	517.44	0.41	0.50	0.56
10t	739.20	0.43	0.50	0.59

5. TGA Data and Analysis

TGA was carried out to measure the thermal stability of HKUST-1 pellets (see Figure S4). The total weight loss of pellets decreases as a function of pressure. The initial weight loss up to 150 °C is assigned to the H_2O desorption resulted from the hydrophilic nature of HKUST-1. The presence of solvent in the sample was confirmed by another weight loss in the range of 200-300 °C, which is assigned to the removal of entrapped DMF from solvothermal synthesis. Finally, the sharp weight loss at ~350 °C in all the samples is corresponding to the structural decomposition of the HKUST-1 framework.

Table S2: Number of DMF molecules (n) trapped in Basolite C300 (HKUST-1) estimated from the TGA data, where $[Cu_3(BTC)_2] \cdot nC_3H_7NO$.

Pellet sample	n
0.5t	-
1t	-
2t	0.24
3t	0.24
5t	0.24
7t	0.19
10t	0.19
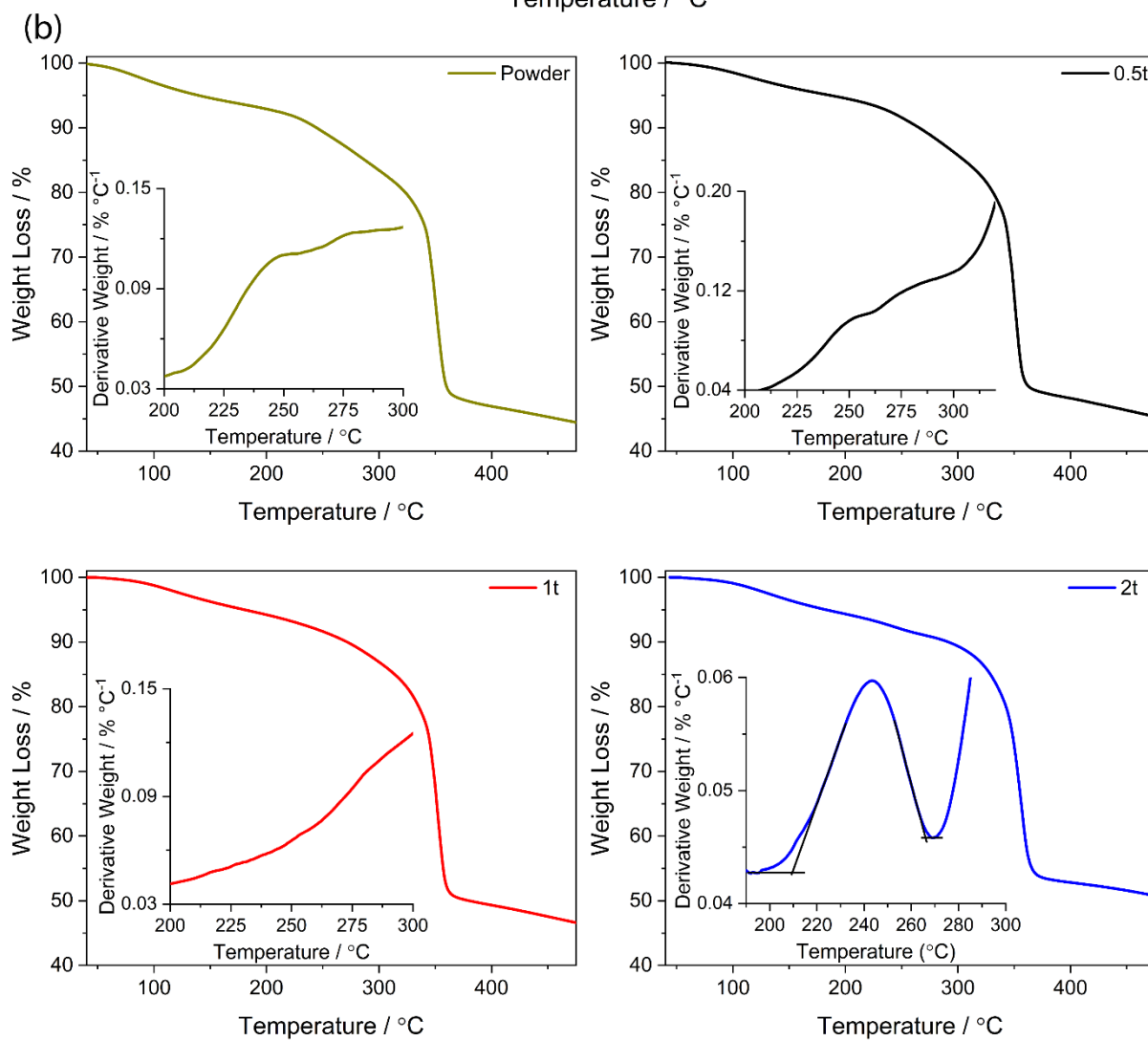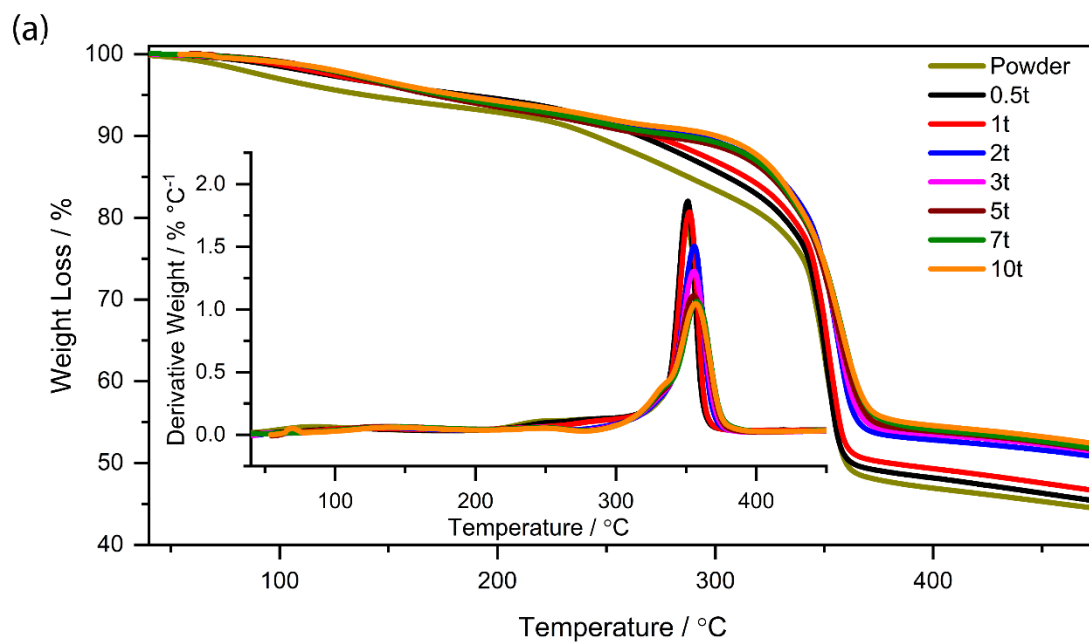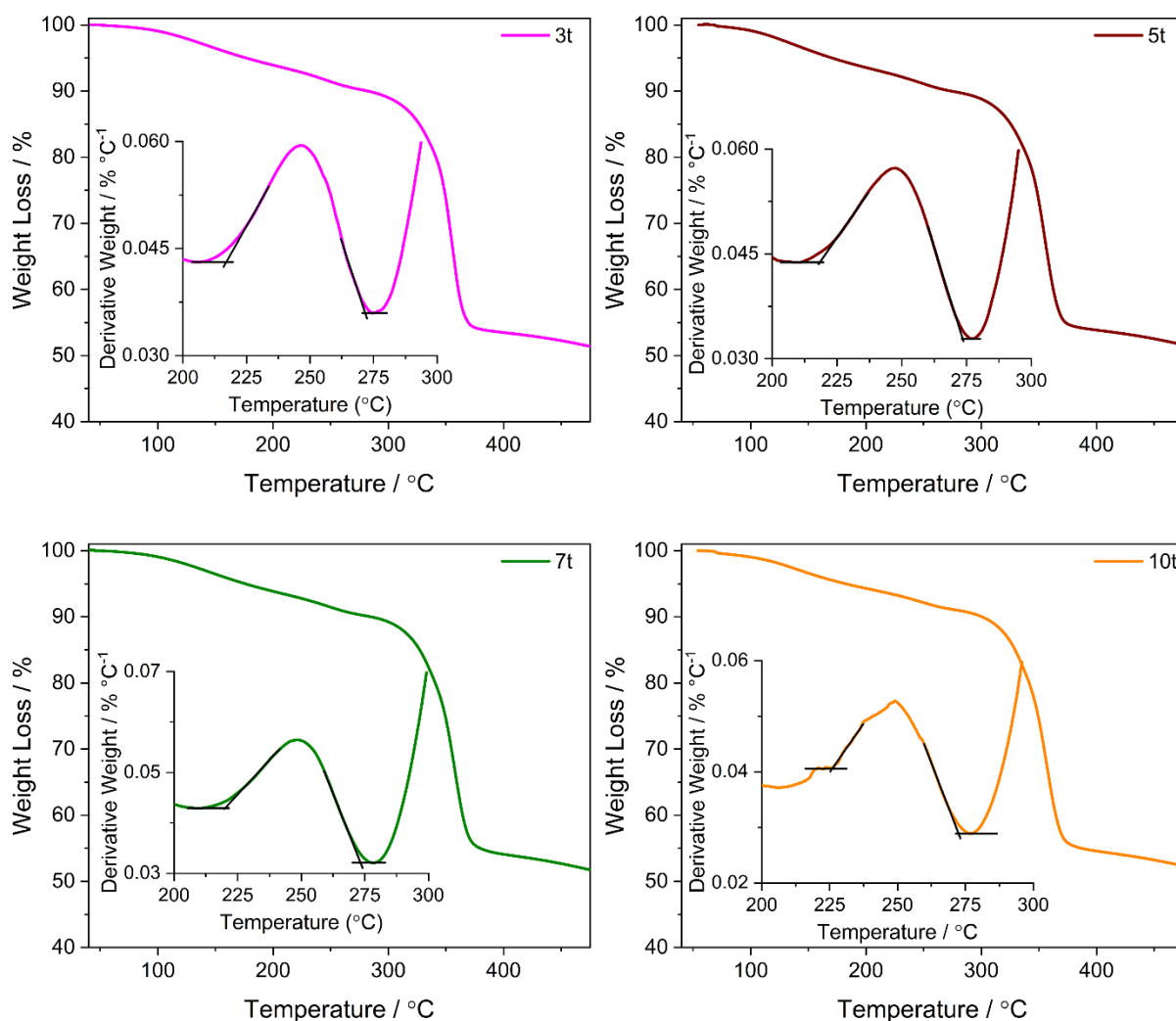
Figure S5: (a) TGA of HKUST-1 samples (Basolite C300) as a function of temperature. Inset shows the derivative weight change as a function of temperature. The hump in the derivative plots (b) of pellets suggest the presence of some DMF molecules from solvothermal synthesis remain trapped in the framework. With the effect of pelleting pressure the weight loss associated with DMF and organic linker becomes more distinctive, which was found overlapped in the pristine powder of HKUST-1.

6. FTIR Data and Analysis

The presence of residual DMF solvent in the MOF framework was further confirmed by the ATR-FTIR spectroscopy shown in Figures S6 and S7. Peaks at 1373 and 1548 cm^{-1} correspond to the C=C stretching whereas 1450 and 1648 cm^{-1} are associated with the symmetric and asymmetric COO stretching, respectively. It can be seen that these peaks broaden with pelleting pressure as a result of amorphization [4]. The peaks at 1260 and 2925 cm^{-1} are assigned to the asymmetric and symmetric C-N stretching, which are related to the trace amount of DMF solvent trapped inside the framework.
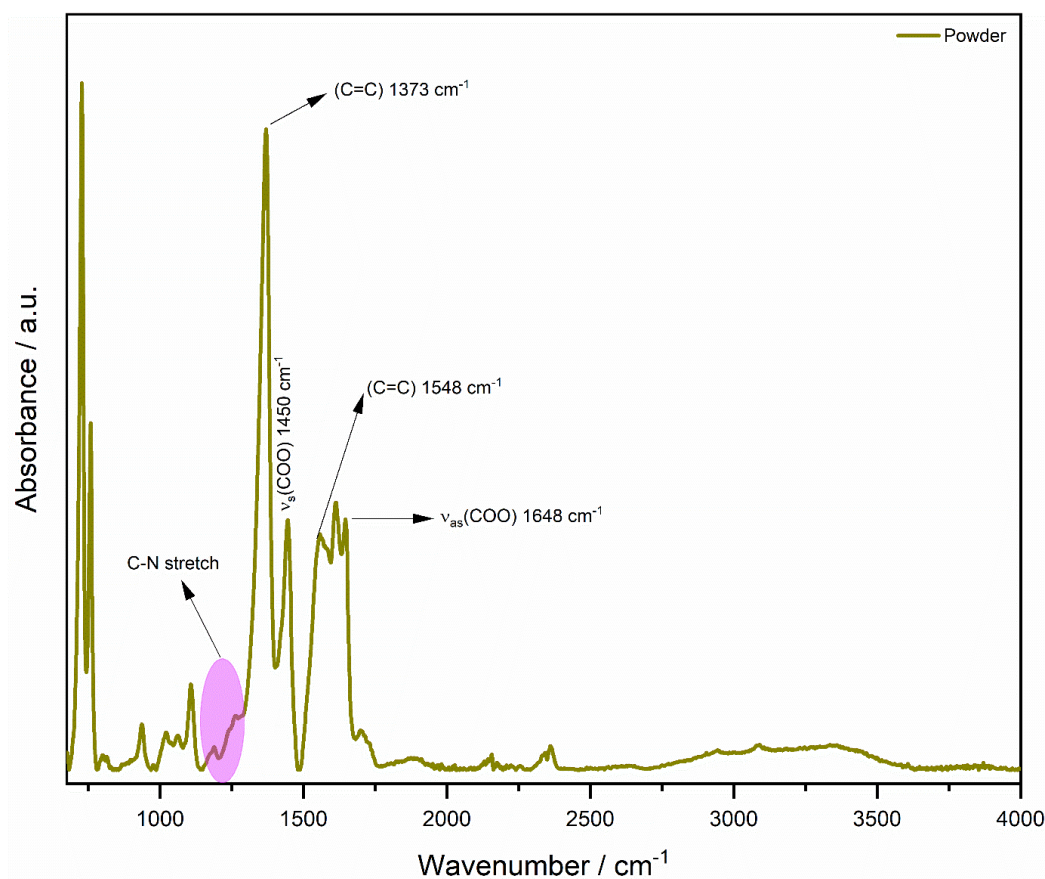
Figure S6: FTIR spectra of HKUST-1 powder. (ν_s=symmetric stretching and ν_{as}=asymmetric stretching).
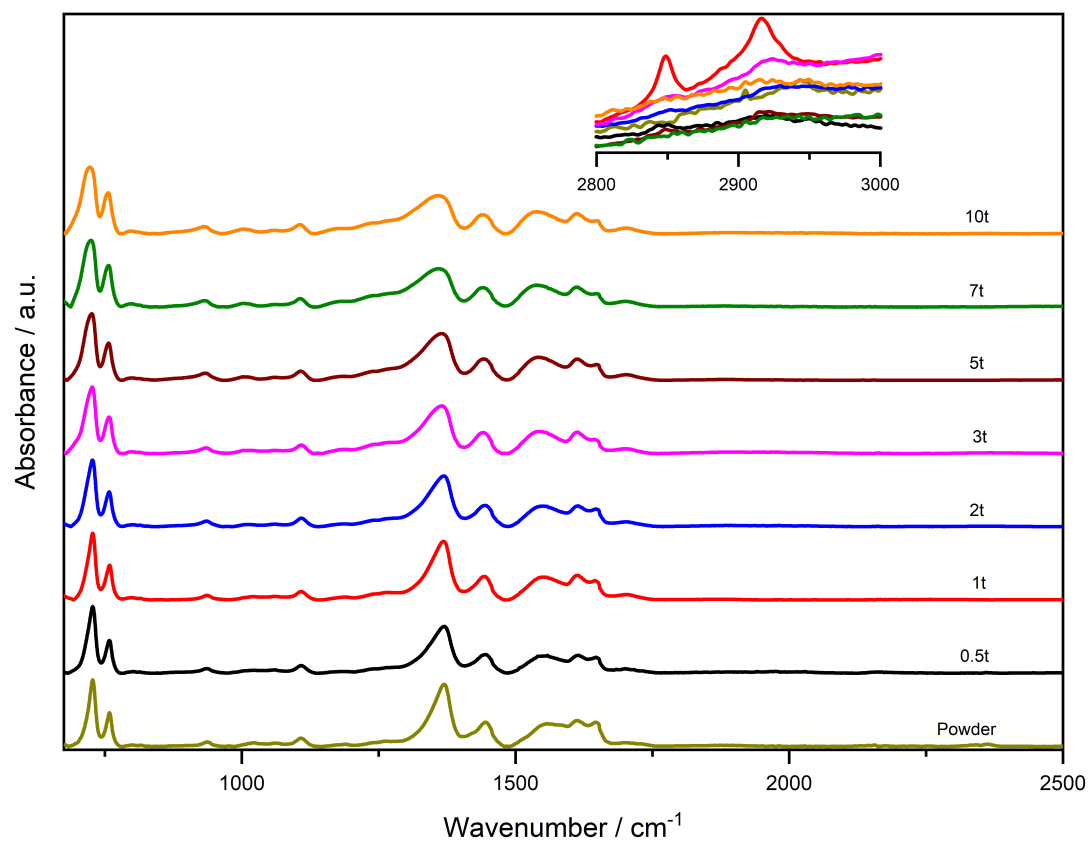
Figure S7: FTIR spectra of HKUST-1 pressure pellets. The inset demonstrates the spectra at higher wavenumber. The frameworks characteristic peaks show broadening with the applying pressure.

7. Real part of dielectric constant in MHz region - Individual pellet dielectrics
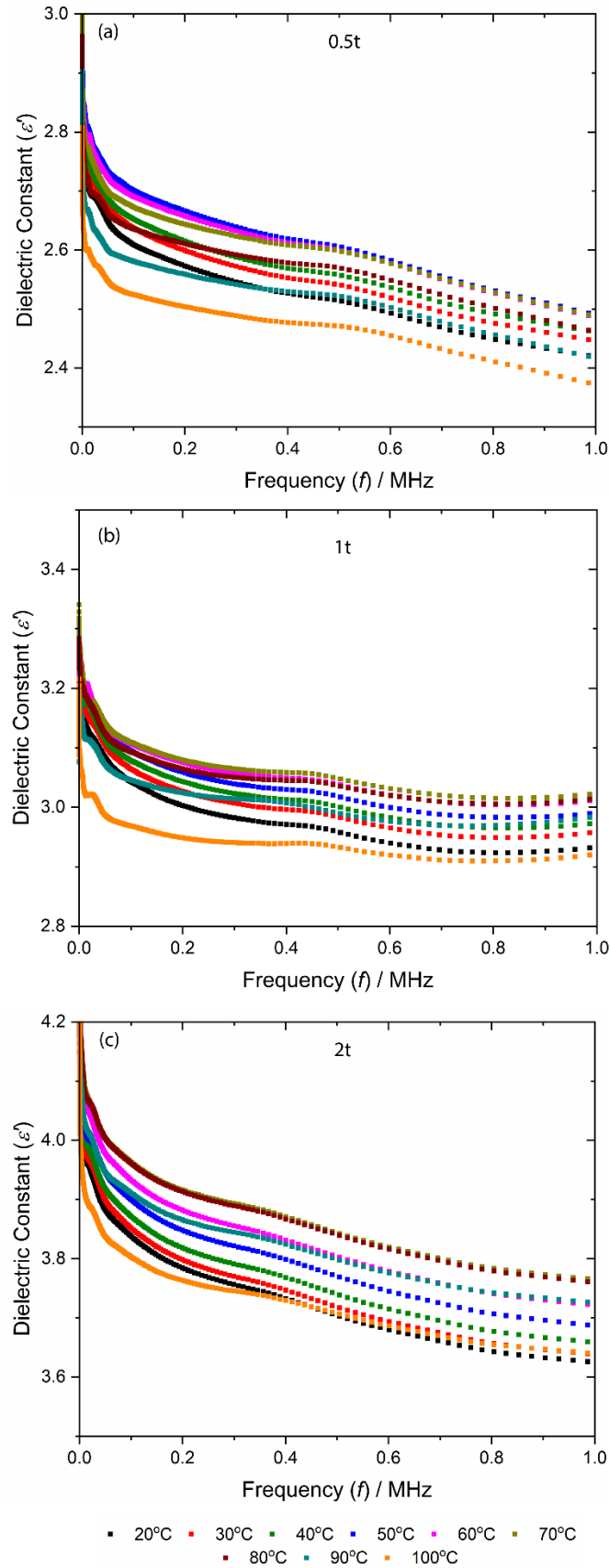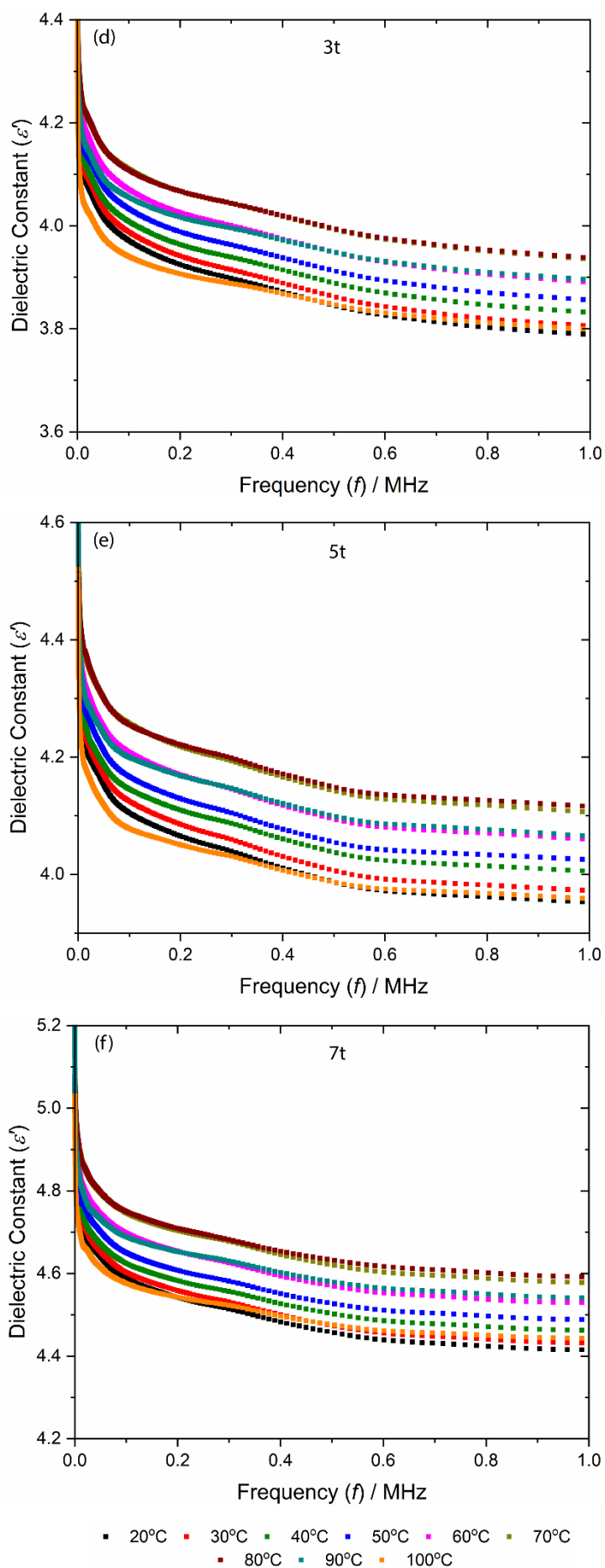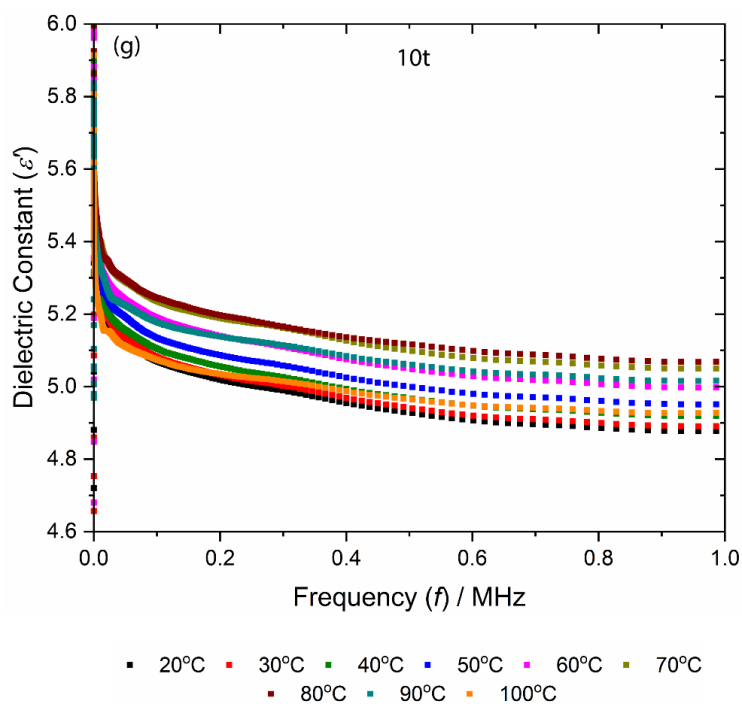
Figure S8: Temperature dependent real part of the dielectric constant as a function of frequency for HKUST-1 pellets prepared under a compression load of: (a) 0.5 ton, (b) 1 ton, (c) 2 ton, (d) 3 ton, (e) 5 ton, (f) 7 ton and (g) 10 ton, corresponding to the pressure of 36.96, 73.92, 147.84, 221.76, 369.60, 517.44 and 739.20 MPa.

8. Imaginary part of dielectric constant in MHz region - Individual pellet dielectrics
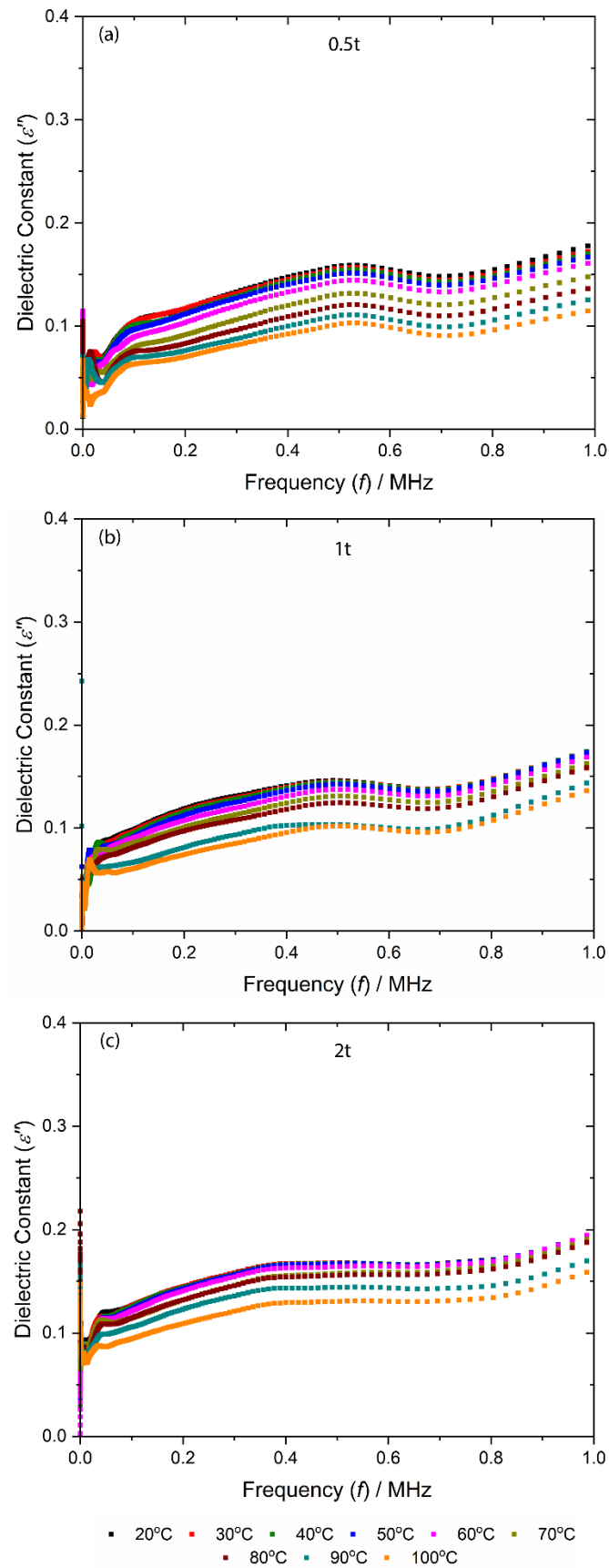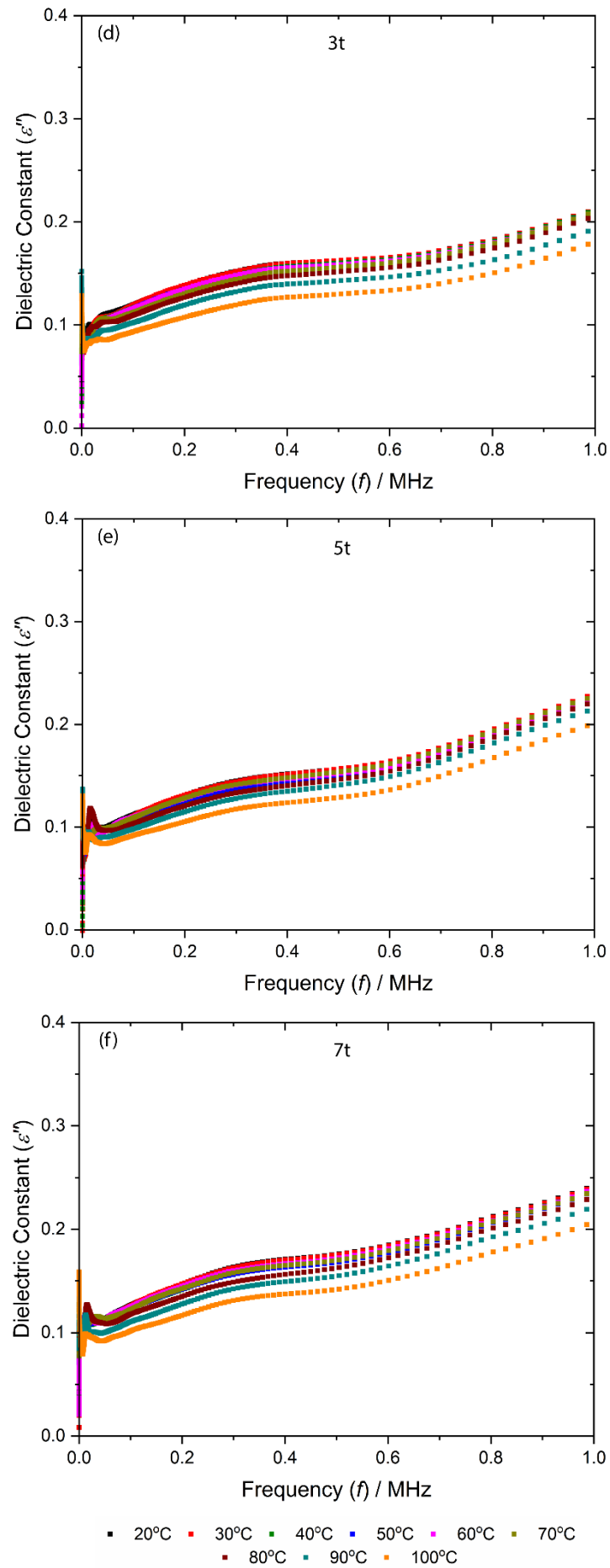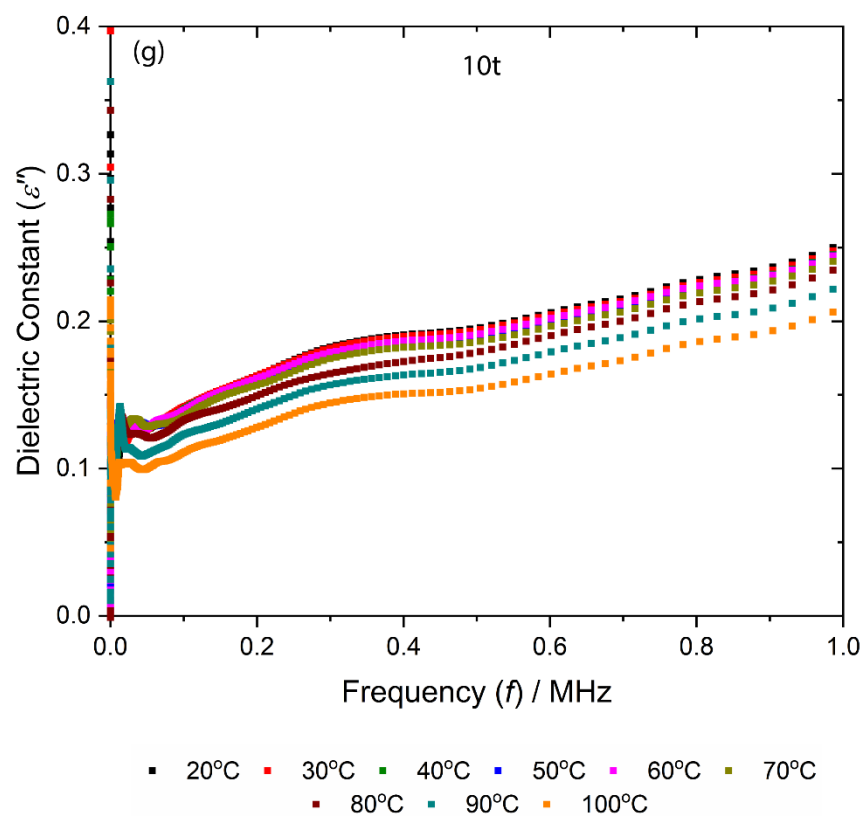
Figure S9: Temperature dependent imaginary part of the dielectric constant as a function of frequency for HKUST-1 pellets prepared under a compression load of: (a) 0.5 ton, (b) 1 ton, (c) 2 ton, (d) 3 ton, (e) 5 ton, (f) 7 ton and (g) 10 ton, corresponding to the pressure of 36.96, 73.92, 147.84, 221.76, 369.60, 517.44 and 739.20 MPa.

9. Loss tangent of dielectric constant in MHz region - Individual pellet dielectrics

(d) 3t

(e) 5t

(f) 7t

Legend: 20°C, 30°C, 40°C, 50°C, 60°C, 70°C, 80°C, 90°C, 100°C
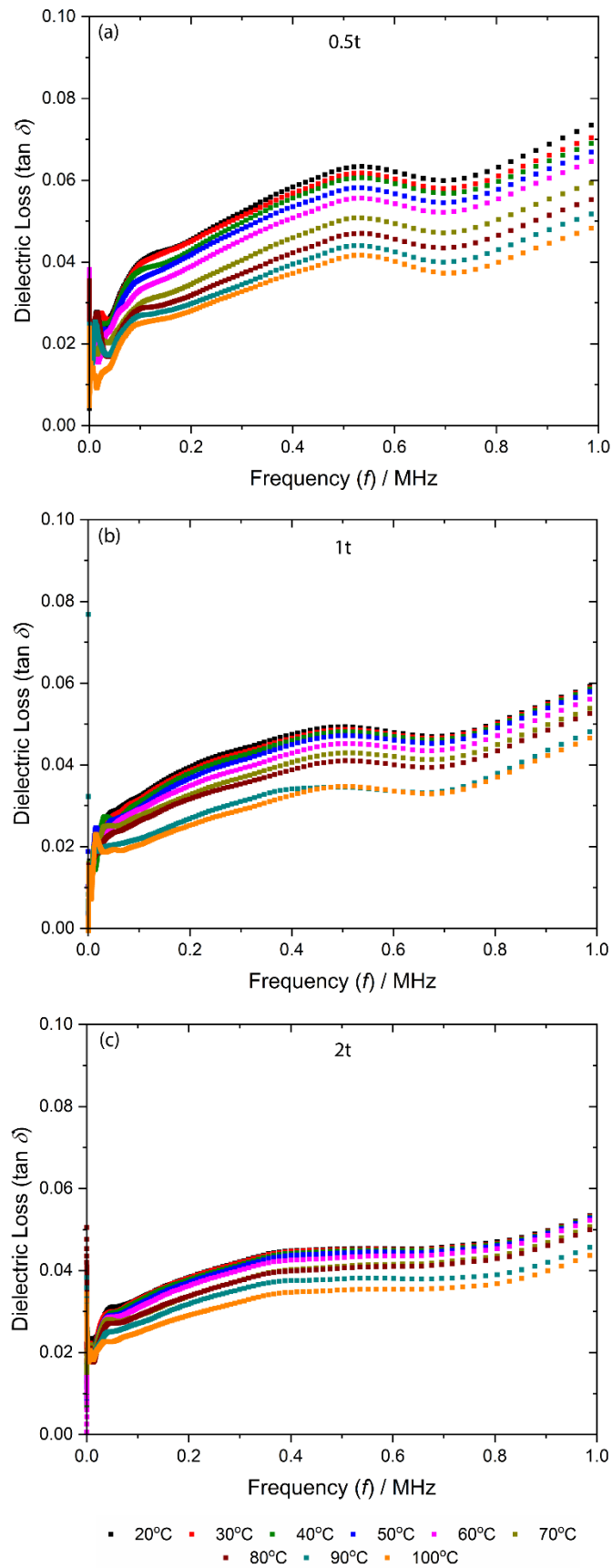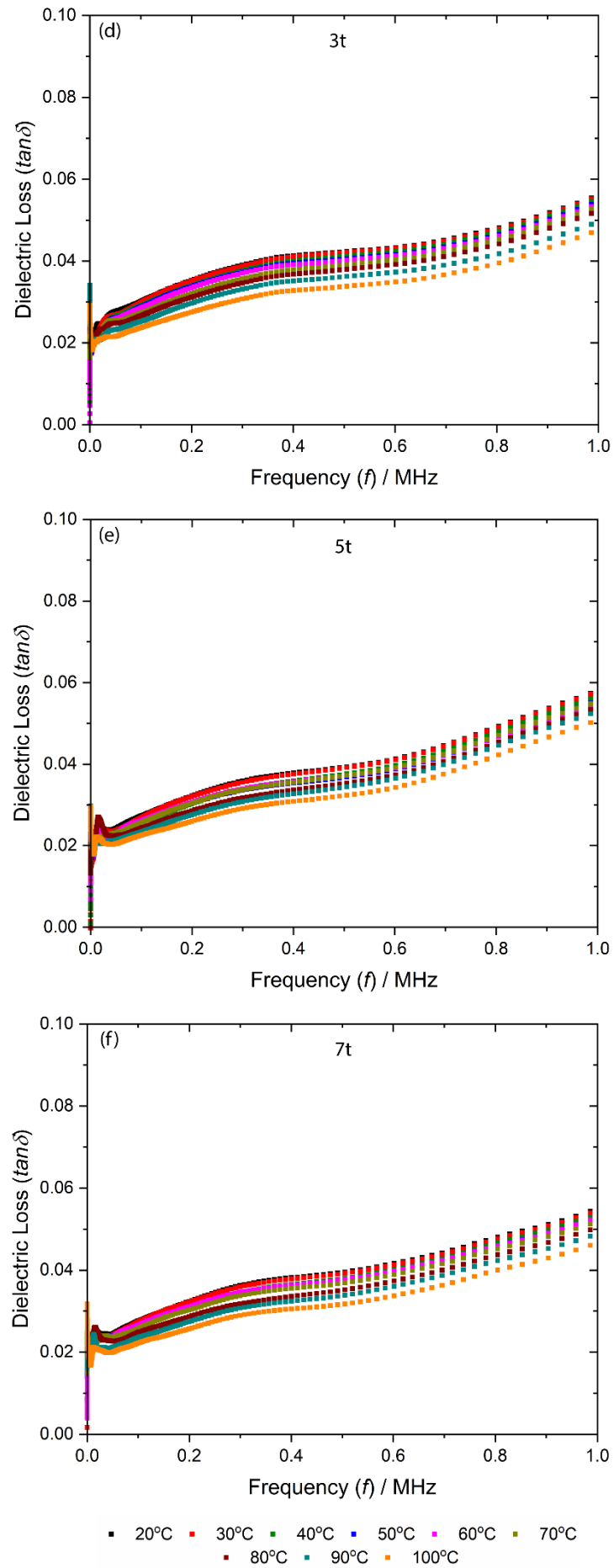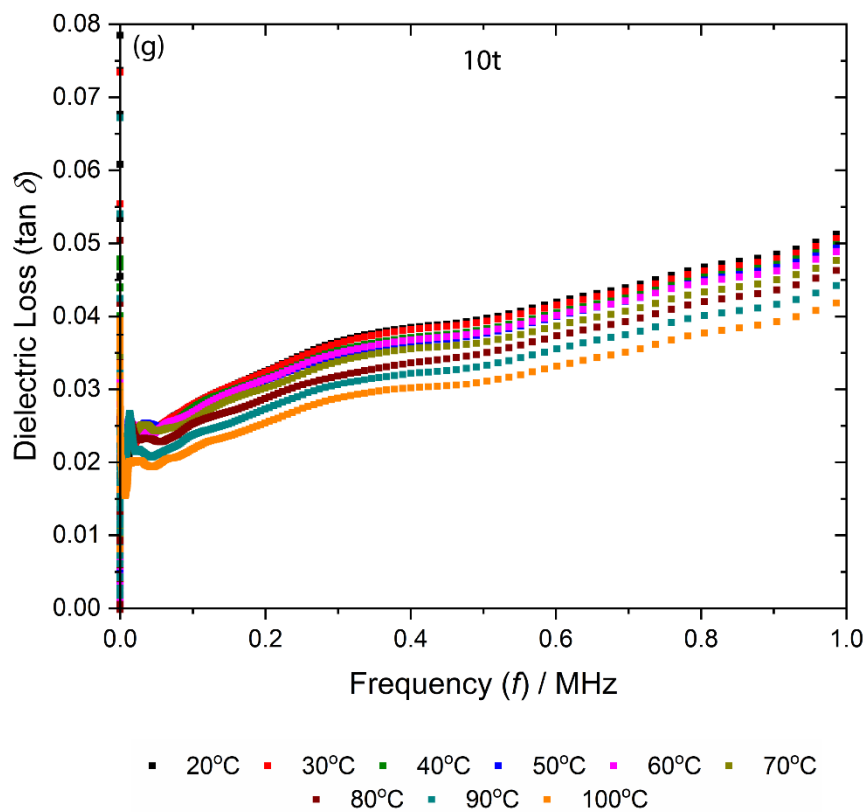
Figure S10: Temperature dependent dielectric loss as a function of frequency for HKUST-1 pellets prepared under a compression load of: (a) 0.5 ton, (b) 1 ton, (c) 2 ton, (d) 3 ton, (e) 5 ton, (f) 7 ton and (g) 10 ton, corresponding to the pressure of 36.96, 73.92, 147.84, 221.76, 369.60, 517.44 and 739.20 MPa.

10. Density functional theory (DFT) calculations of dielectric properties

Density functional theory (DFT) calculations were performed using the CRYSTAL17 code [5]. We used the B3LYP hybrid exchange-correlation functional [6] augmented with two- and three-body corrections for dispersive interactions [7] *i.e.* B3LYP-D3(ABC). We employ the triple-zeta (TZP) quality basis sets: Cu and C are pob-TZVP, O and H are Alhrichs TVZP basis set [8]. The tolerances for the one- and two-electrons integrals calculation were set to 10^{-7} and 10^{-7} for the Coulomb series, and to 10^{-7}, 10^{-7} and 10^{-25} for the Exchange series. All calculations (including geometry optimization and frequency calculation) were performed with a threshold of 10^{-10} Ha for the self-consistent field (SCF) process. Furthermore, the shrinking factors for the diagonalization of the Kohn-Sham matrix in the reciprocal space has been set to 2 for the Monkhorst-Pack and 2 for the Gilat nets corresponding to 3 **k**-points for the high symmetry HKUST-1 and 4 **k**-points for the low symmetry system (see below).

An ideal (defect free) HKUST-1 framework structure with ferromagnetic cubic symmetry (*Fm*-3*m*) was geometrically optimized in accordance with ref. [9]. All the calculations have been performed with the constraints imposed by the symmetry.

For the optimized structure, the reflectance spectrum and the complex dielectric function at 0 K were predicted. The real and imaginary parts of the dielectric function were obtained through Kramers-Kronig relations [10] and plotted as the ε' and ε'' values as a function of frequency.

The complete CRYSTAL input file for the vibrational frequencies calculation including the reflectance spectrum of the optimized structure of an ideal HKUST-1 is reported below.

```
HKUST-1 ferromagnetic B3LYP-D* BS: H,O TZP; C,Cu pob-TZVP
CRYSTAL
0 0 0
225
26.25044014
6
29   -2.156467442391E-01 -2.156467442391E-01  0.000000000000E+00
 8   -1.833615509381E-01 -2.562918895929E-01 -5.237261654586E-02
 6   -1.784366326101E-01 -3.215633673899E-01 -1.138043804763E-01
 6   -2.032673129463E-01 -2.967326870537E-01 -6.962742207363E-02
 6   -1.353121864950E-01 -2.999565071966E-01 -1.353121864950E-01
 1    1.189659997482E-01 -1.189659997482E-01  2.659154056390E-01
FREQCALC
NUMDERIV
2
```

```
INTENS
INTCPHF
ENDCPHF
IRSPEC
REFRIND
DIELFUN
DAMPFAC
0.5
GAUSS
ENDIR
END
END
29 14
0 0 8 2.0 1.0
 377518.79923 0.00022811766128
 56589.984311 0.00176880359310
 12878.711706 0.00919934602270
 3645.3752143 0.03741101643400
 1187.0072945 0.12189873737000
 426.46421902 0.28983900714000
  165.70660164 0.41531872174000
 65.598942707 0.21905799287000
0 0 4 2.0 1.0
 414.41265811 -0.02468252505300
 128.32056039 -0.11716827406000
 20.622089750 0.55301315941000
 8.7821226045 0.52242718609000
0 0 2 2.0 1.0
 13.741372006 -0.22736061821000
 2.2431246833 0.71761210873000
0 0 1 1.0 1.0
 0.8152953200 1.00000000000000
0 0 1 0.0 1.0
 0.4076476600 1.00000000000000
0 0 1 0.0 1.0
 0.1768011100 1.00000000000000
0 2 6 6.0 1.0
 2034.7596692 0.00235248222980
 481.90468106 0.01913407075100
 154.67482963 0.09017110527800
 57.740576969 0.26063284735000
 23.099052811 0.42093485770000
 9.3882478591 0.24344615121000
0 2 3 6.0 1.0
 37.596171210 -0.02899109453000
 5.1240690810 0.54919083831000
 2.0119996085 0.93793330488000
0 2 1 0.0 1.0
 1.4641814000 1.00000000000000
0 2 1 0.0 1.0
 0.7320907000 1.00000000000000
0 3 4 10.0 1.0
 74.129460637 0.01436321667600
 21.359842587 0.08662817709600
 7.4995240537 0.25631430541000
 2.7601394169 0.40374062368000
0 3 1 0.0 1.0
```

```
 1.4592938300 1.00000000000000
0 3 1 0.0 1.0
 0.6355722500 1.00000000000000
0 4 1 0.0 1.0
 2.2330000000 1.00000000000000
6 8
0 0 6 2.0 1.0
13575.349682 0.00022245814352
2035.2333680 0.00172327382520
463.22562359 0.00892557153140
131.20019598 0.03572798450200
42.853015891 0.11076259931000
15.584185766 0.24295627626000
0 0 2 2.0 1.0
6.2067138508 0.41440263448000
2.5764896527 0.23744968655000
0 0 1 0.0 1.0
0.4941102000 1.00000000000000
0 0 1 0.0 1.0
0.1644071000 1.00000000000000
0 2 4 2.0 1.0
34.697232244 0.00533336578050
7.9582622826 0.03586410909200
2.3780826883 0.14215873329000
0.8143320818 0.34270471845000
0 2 1 0.0 1.0
0.5662417100 1.00000000000000
0 2 1 0.0 1.0
0.2673545000 1.00000000000000
0 3 1 0.0 1.0
0.8791584200 1.00000000000000
1 4
0 0 3 1.0 1.00
  34.0613410        0.602519780E-02
   5.12357460       0.450210940E-01
   1.16466260       0.201897260
0 0 1 0.0 1.00
   0.327230410      1.00000000
0 0 1 0.0 1.00
   0.103072410      1.00000000
0 2 1 0.00 1.00
   0.8000000000D+00  0.1000000000D+01
8 10
0 0 5 2.0 1.00
     15902.6475       0.514998037E-03
     2384.95378       0.398197644E-02
     542.719572       0.204769719E-01
     153.404079       0.802623679E-01
     49.5457161       0.237668399
0 0 1 2.0 1.00
     17.3396499       1.00000000
0 0 1 0.0 1.00
     6.33033553       1.00000000
0 0 1 0.0 1.00
     1.69958822       1.00000000
0 0 1 0.0 1.00
    0.689544913       1.00000000
```

```
0 0 1 0.0 1.00
      0.239360282       1.00000000
0 2 4 4.0 1.00
      63.2705240        0.607092060E-02
      14.6233123        0.419476887E-01
      4.44895180        0.161568840
      1.52815132        0.356827793
0 2 1 0.0 1.00
      0.529973159       1.00000000
0 2 1 0.0 1.00
      0.175094460       1.00000000
0 3 1 0.00 1.00
      0.1200000000D+01  0.1000000000D+01
99 0
END
DFT
B3LYP-D3
XXLGRID
SPIN
END
TOLINTEG
7 7 7 7 25
SHRINK
2 2
SPINLOCK
12
50
TOLDEE
10
DFTD3
ABC
END
END
```

The pressure-dependent dielectric calculations at 190 MPa and 360 MPa were carried out by a two-step procedure. First, we run a series of constant-volume geometry optimization and then the data were fitted with a Birch-Murnagham (BM) equation of state. Second, the cell volume was fixed at the pressure corresponding to 190 MPa and 360 MPa as obtained from the BM fitting. Finally, vibrational frequencies and dielectric response were computed as described above. Note that the present calculations show that at 360 MPa the cubic structure is no longer stable and a phase transition occurs toward a lower symmetry tetragonal phase. Therefore, the reported results at 360 MPa correspond to the tetragonal unit cell.

11. Reflectivity spectra *R(ω)* in the far-IR and mid-IR regions
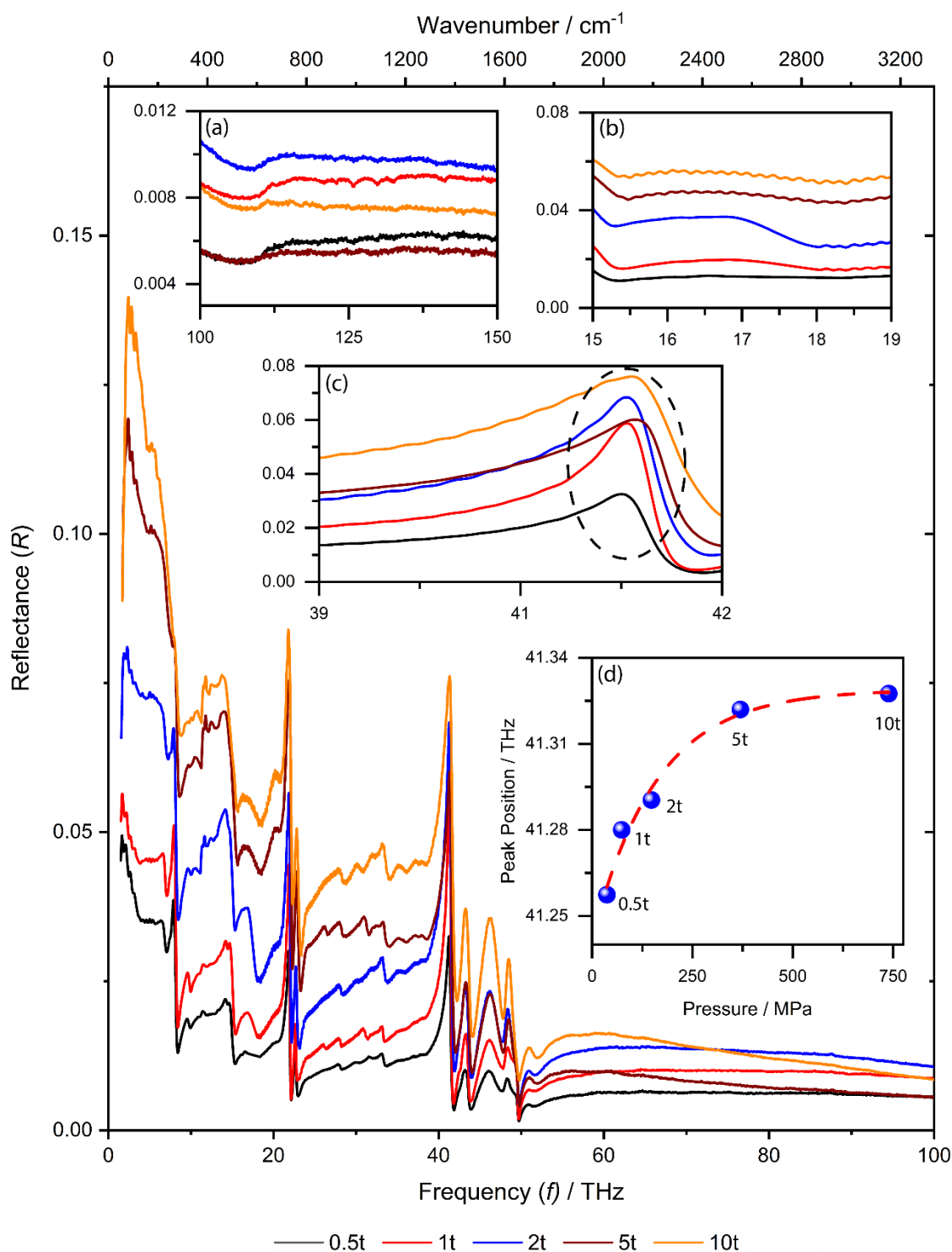
Figure S11: Reflectance spectra of HKUST-1 pellets. Inset: (a) reflectivity spectra from 100 - 150 THz, (b) both far-IR and mid-IR spectra are joined together at 600 cm^{-1} (~18 THz), (c) and (d) shows the blue shift of peaks as a function of the pelleting pressure. The peak positions were identified using the Gaussian fit.

12. Real part of dielectric constant in THz region: Experiments vs DFT
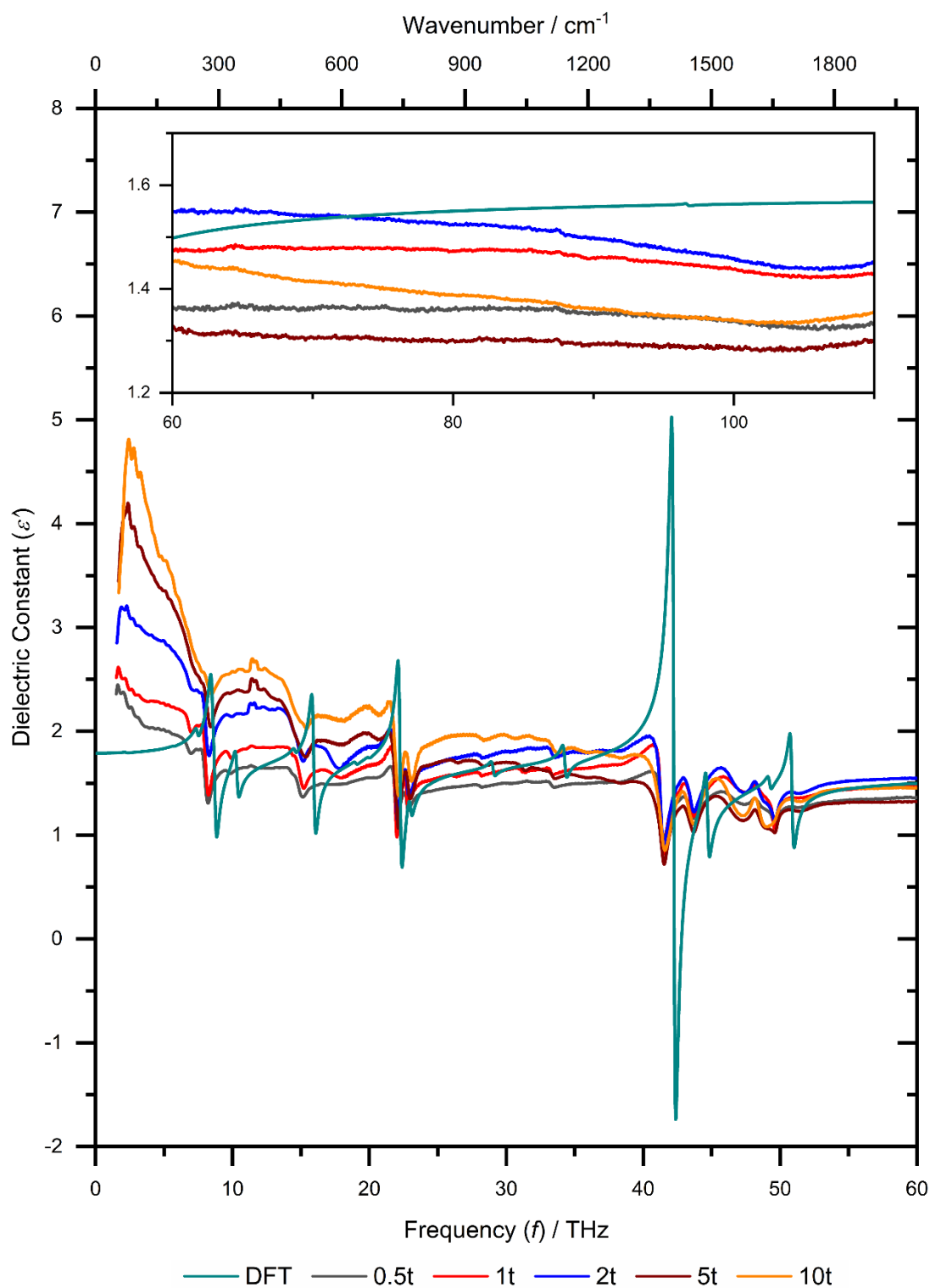
Figure S12: Overlapped experimental and simulated DFT spectra for the real part of dielectric constant as a function of frequency. The DFT calculation predicted all the oscillatory transitions in the HKUST-1 dielectric spectra. Inset shows the dielectric spectra at higher frequencies up to 150 THz.

13. Imaginary part of dielectric constant in THz region - experiments vs DFT
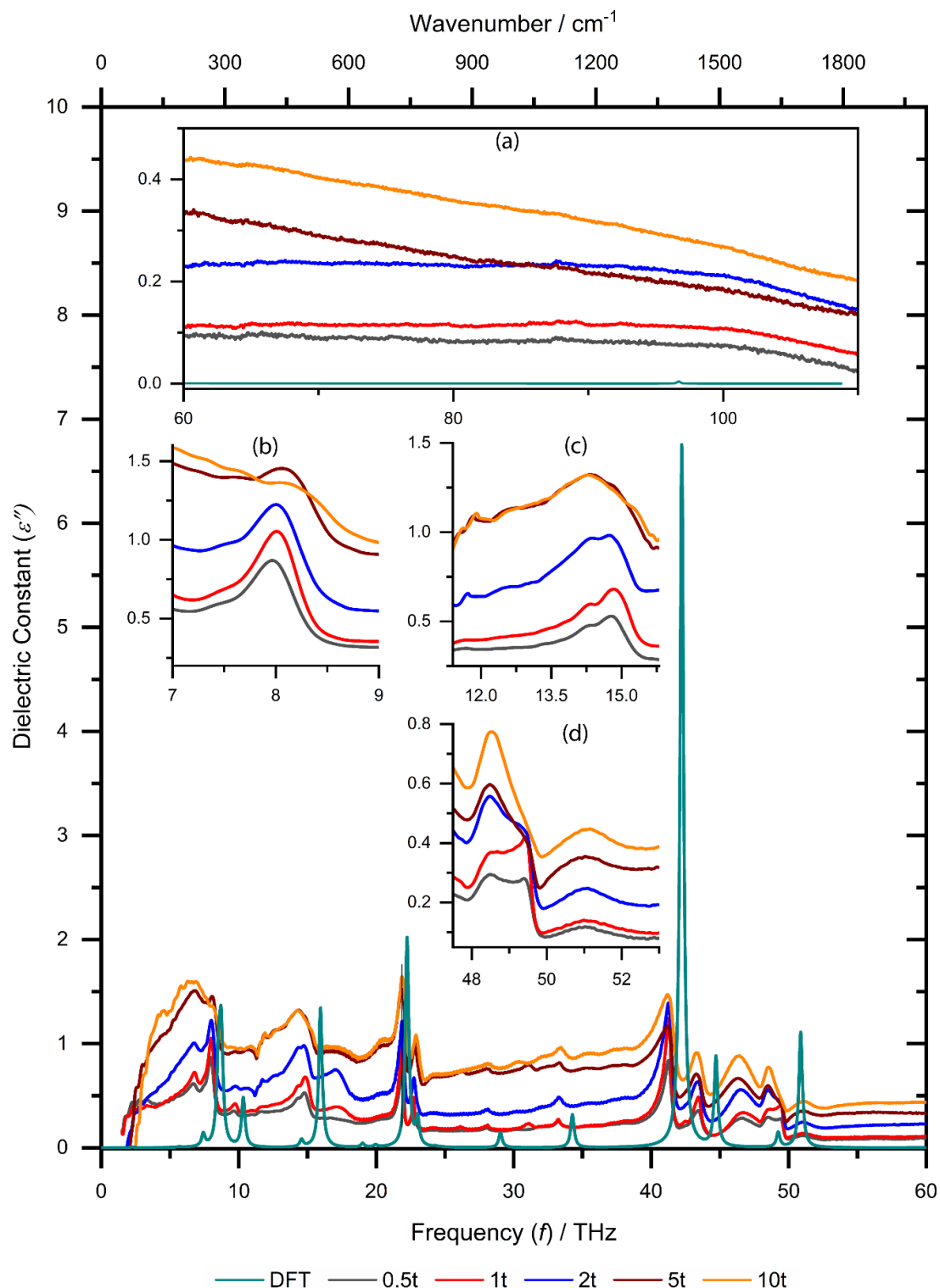
Figure S13: Overlapped experimental and simulated DFT spectra for the imaginary part of dielectric constant. Inset (a) shows the dielectric spectra at higher frequencies. The DFT calculation predicted all the oscillatory transitions in the frequency-dependent dielectric

spectra of HKUST-1. Interestingly, all the modes in the experimental data are slightly in the left side of the DFT simulated spectra. Inset (b) blue shift in the Cu-paddle wheel deformation mode (O-Cu-O bending and Cu-Cu buckling at 8 THz), with applying pressure, whereas inset (c) show the red shift in modes related to the linker deformation (out-of-plane aromatic ring deformation). Inset (d) demonstrate the blue shift in the mode associated with the Cu-O stretching.

14. Loss tangent (tan δ) of HKUST-1 in MHz and THz regions
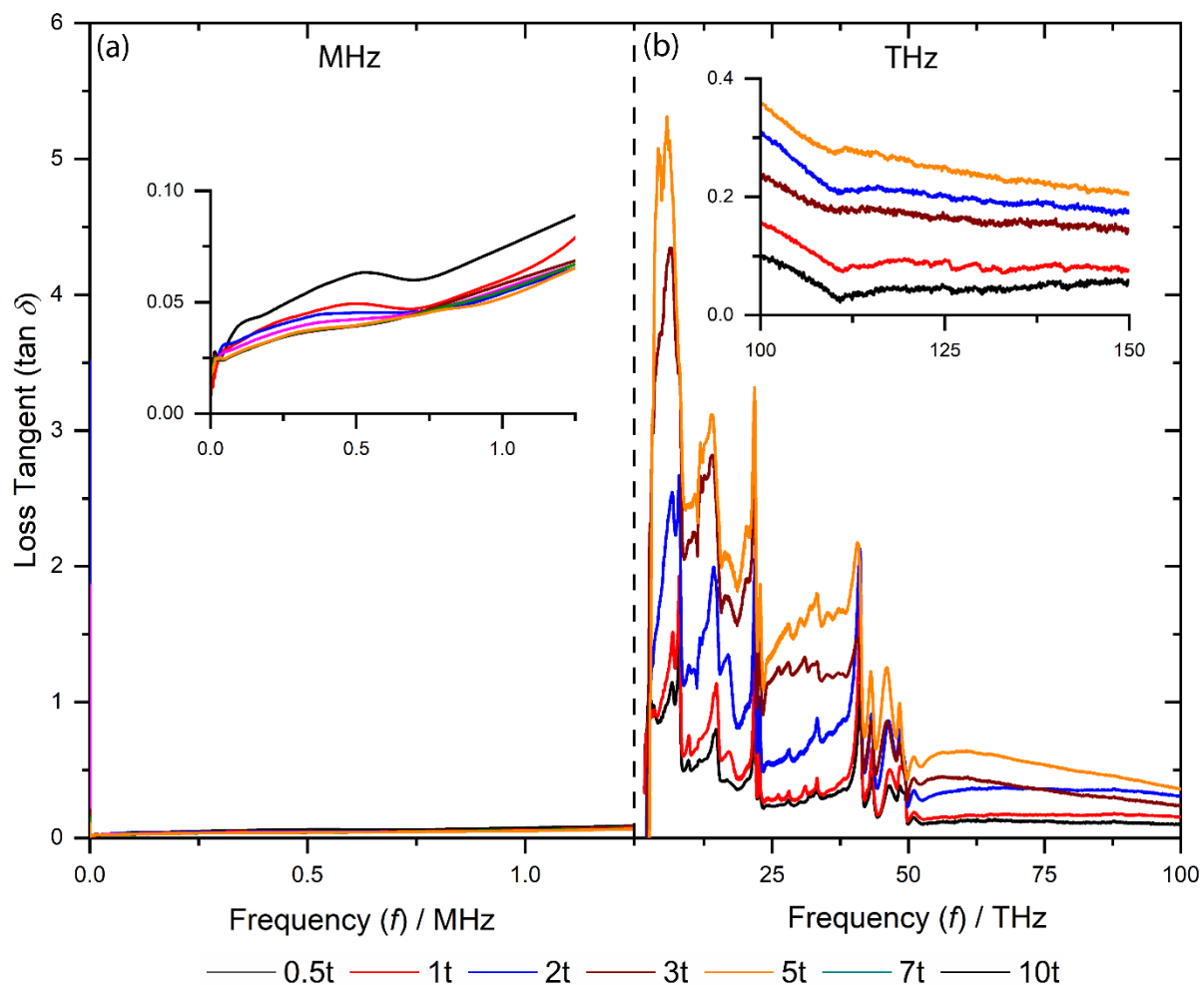
Figure S14: Dielectric loss tangent spectra of pellets in the MHz and THz region. The left inset shows the zoomed view of pellets in the MHz region, whereas right inset shows the extended dataset up to 150 THz.

15. Pressure-dependent DFT calculations

15.1 Components of the complex refractive index, *n* + *iκ*
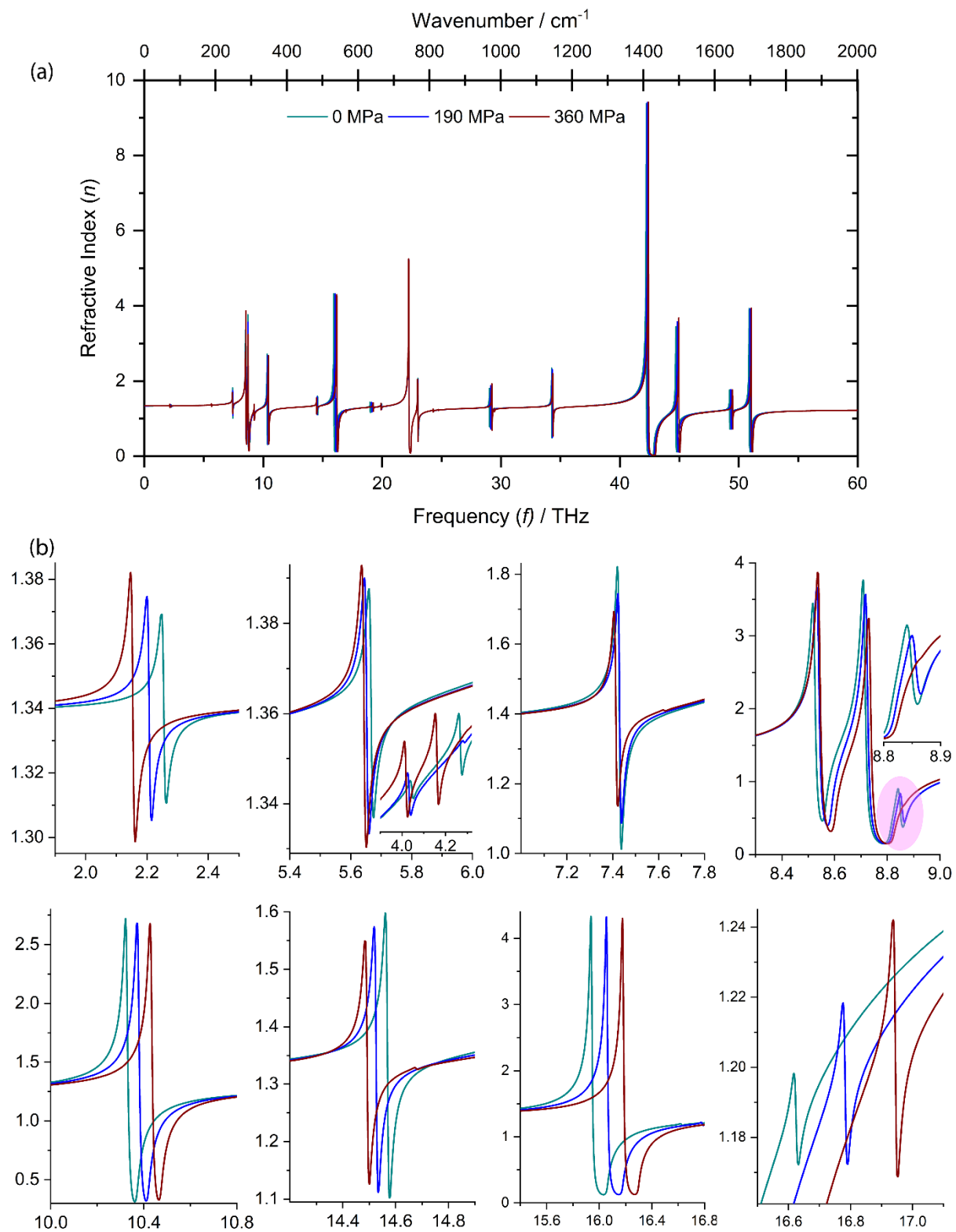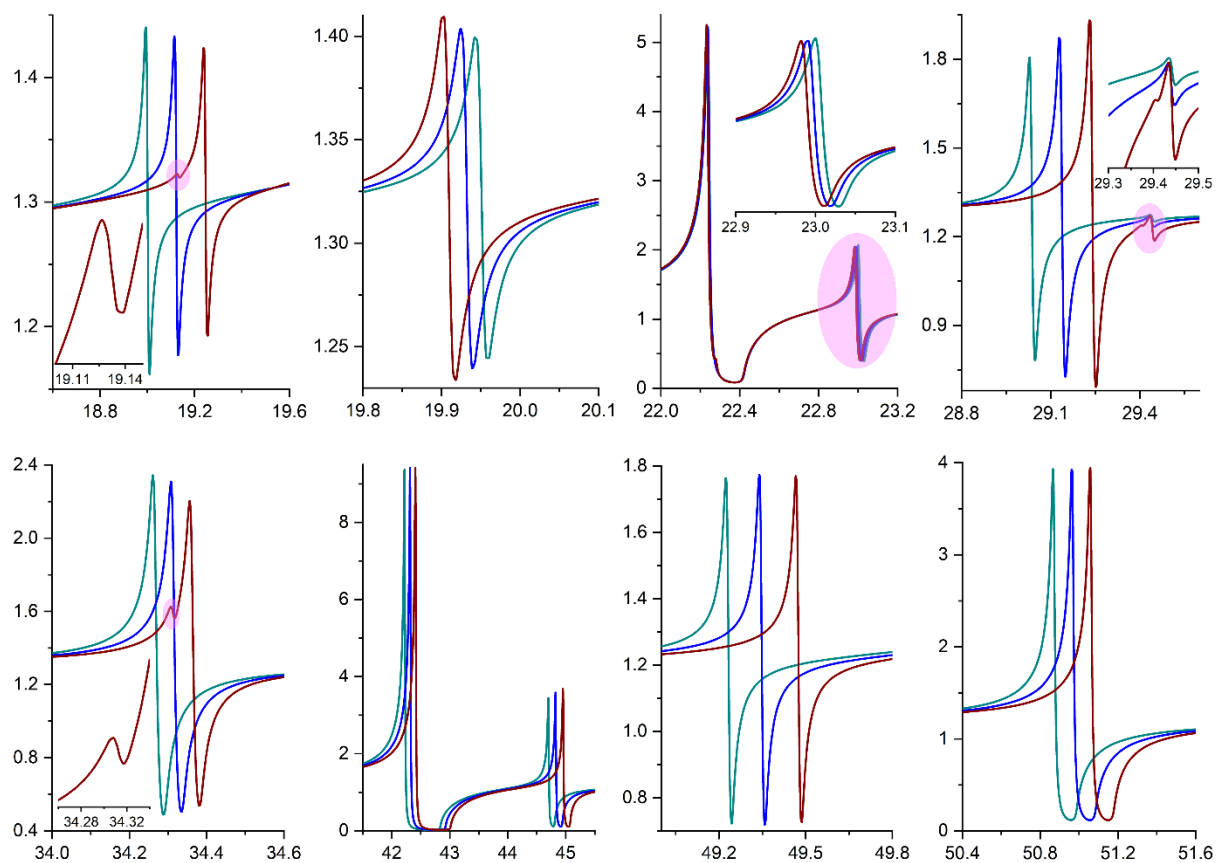
Figure S15: Pressure-dependent refractive index calculated by DFT. (a) Real part of the refractive index *n*. (b) Zoomed plots of the selected frequencies showing the red/blue shifts.

(a)

(b)
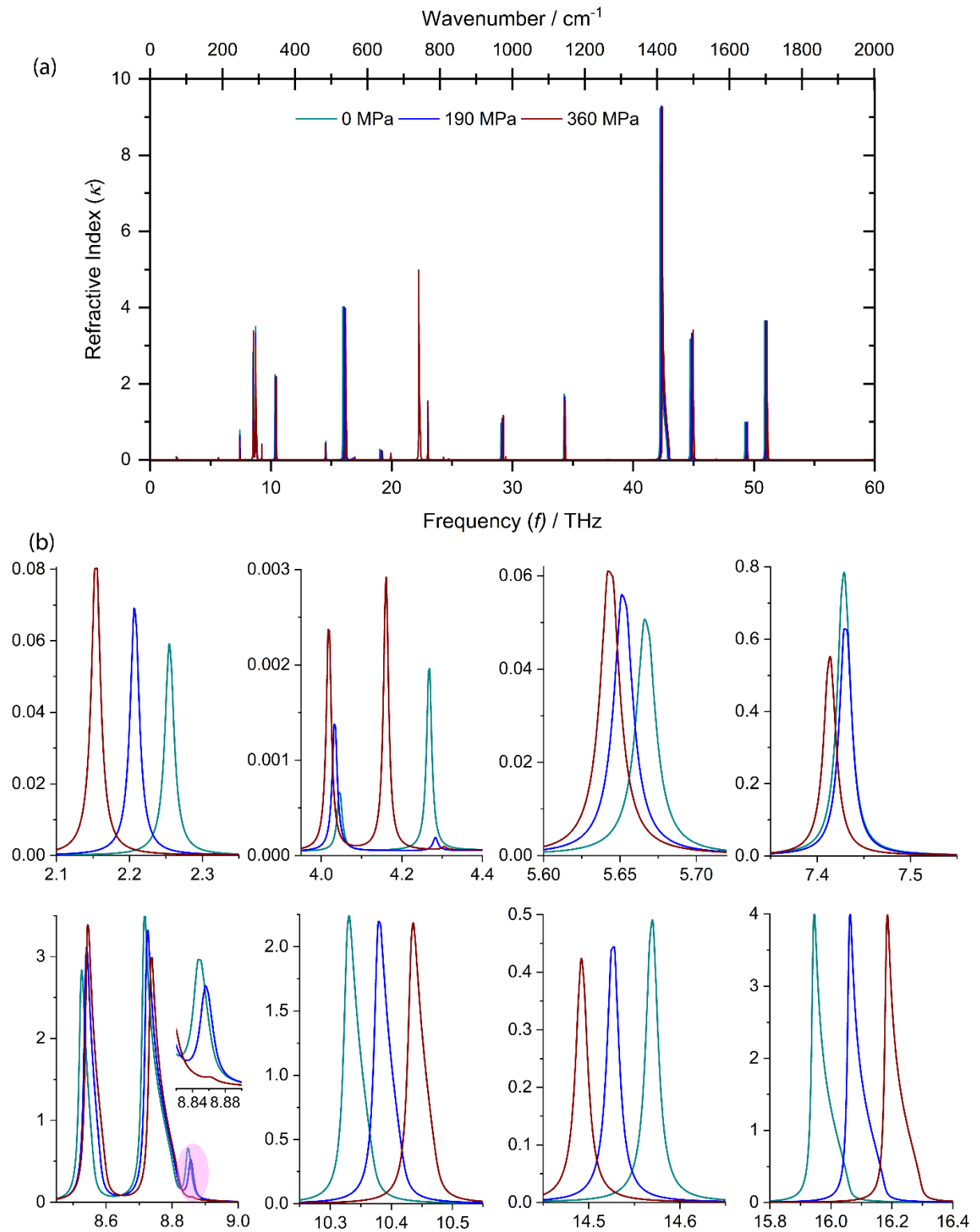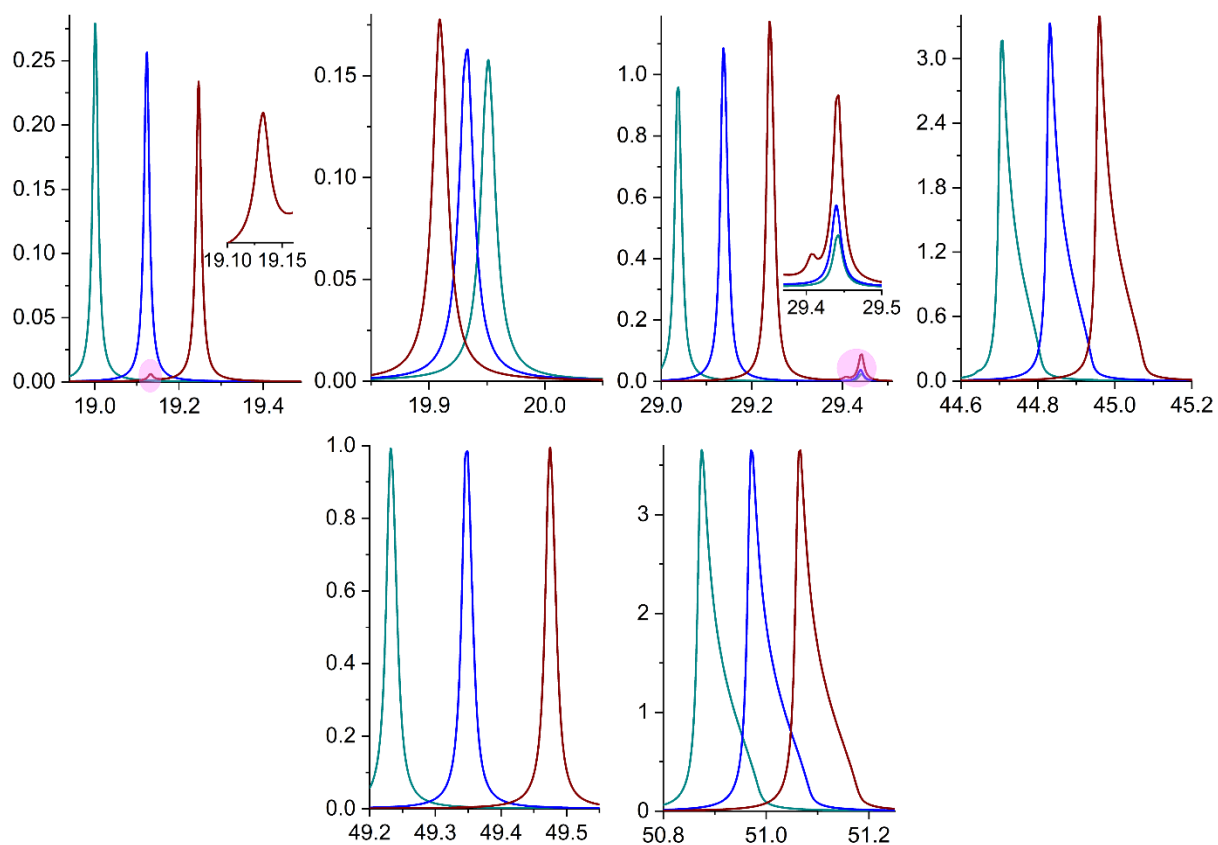
Figure S16: Pressure-dependent refractive index calculated by DFT. (a) Imaginary part of the refractive index, κ. (b) Zoomed plots of the selected frequencies showing the red/blue shifts.

15.2 Components of the complex dielectric property, $\varepsilon' + i\varepsilon''$
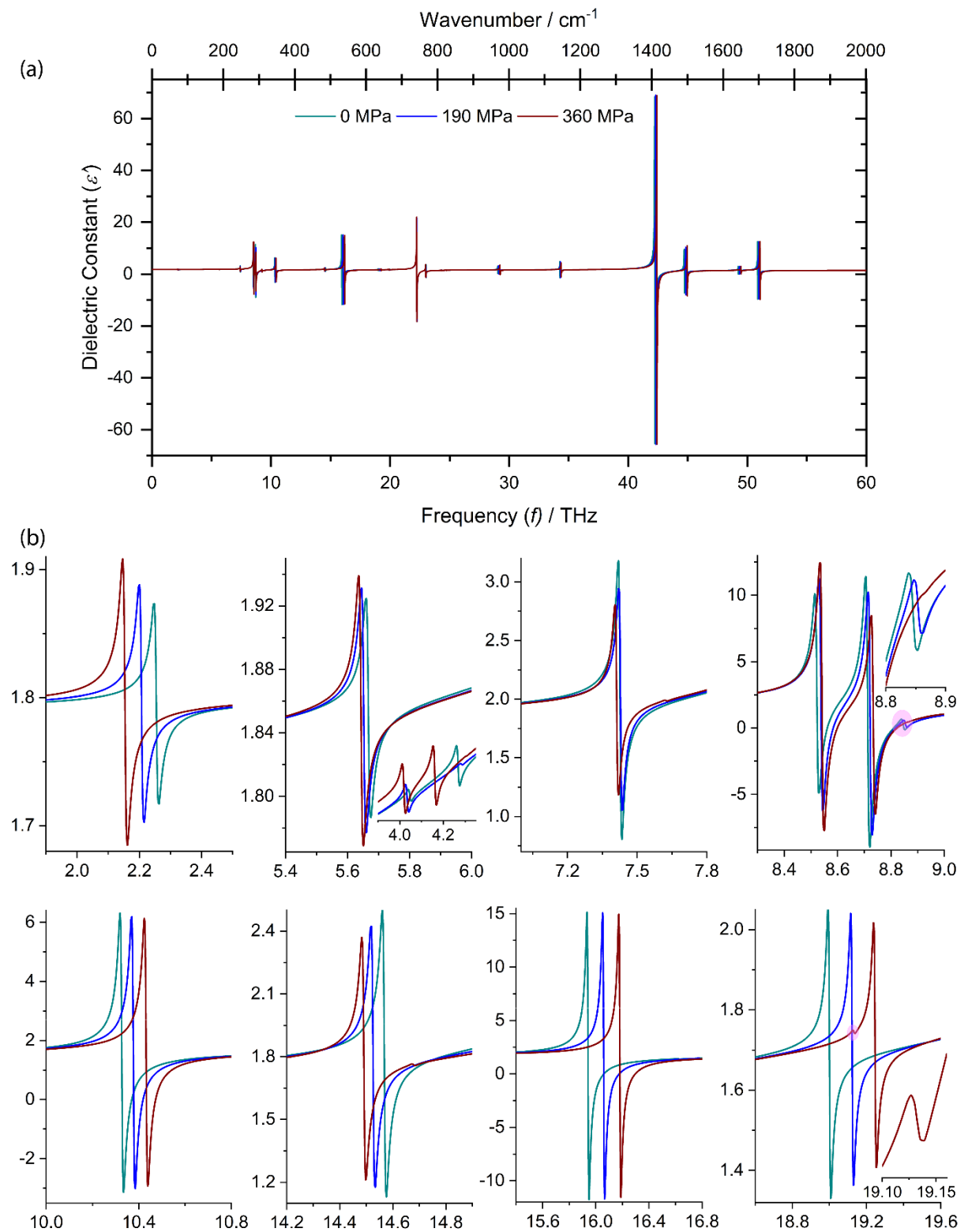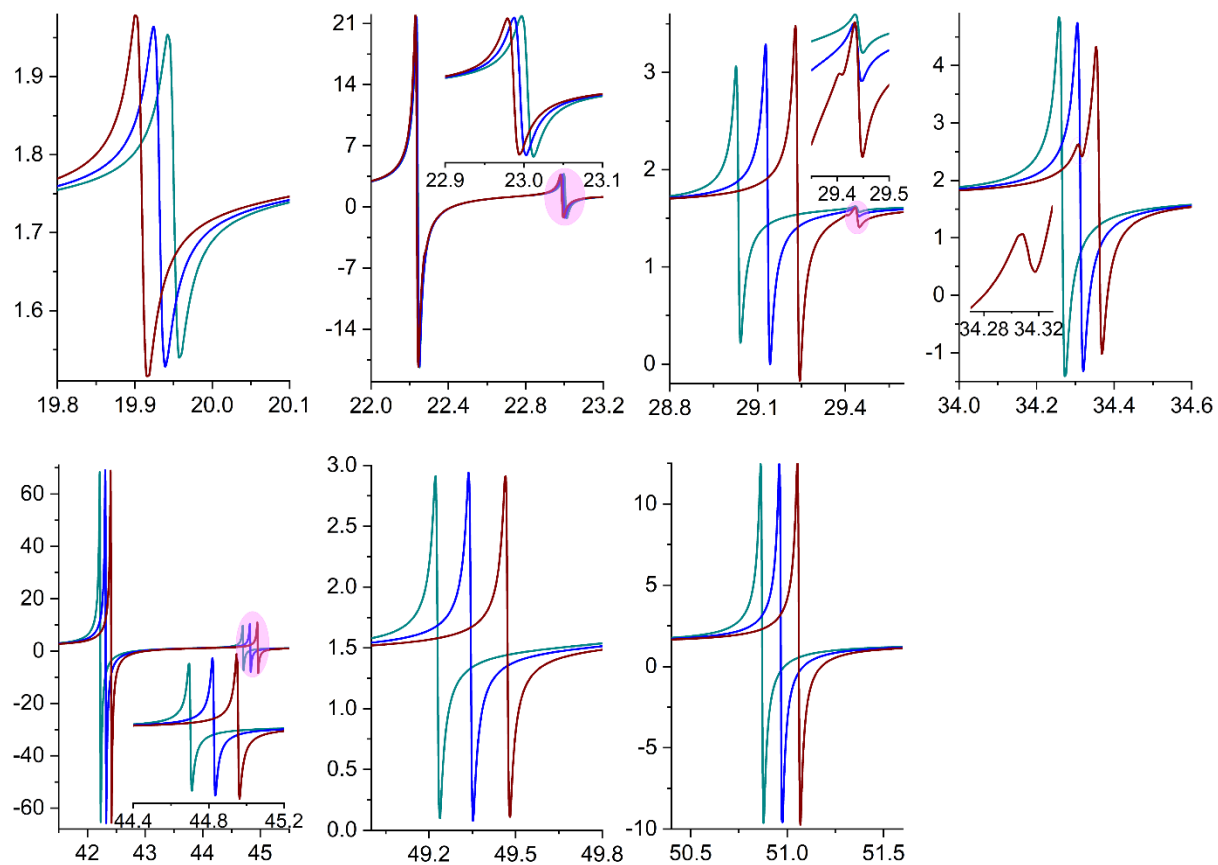
Figure S17: Pressure-dependent dielectric constant calculated by DFT. (a) Real part of the dielectric constant ε'. (b) Zoomed plots of the selected frequencies showing the red/blue shifts.
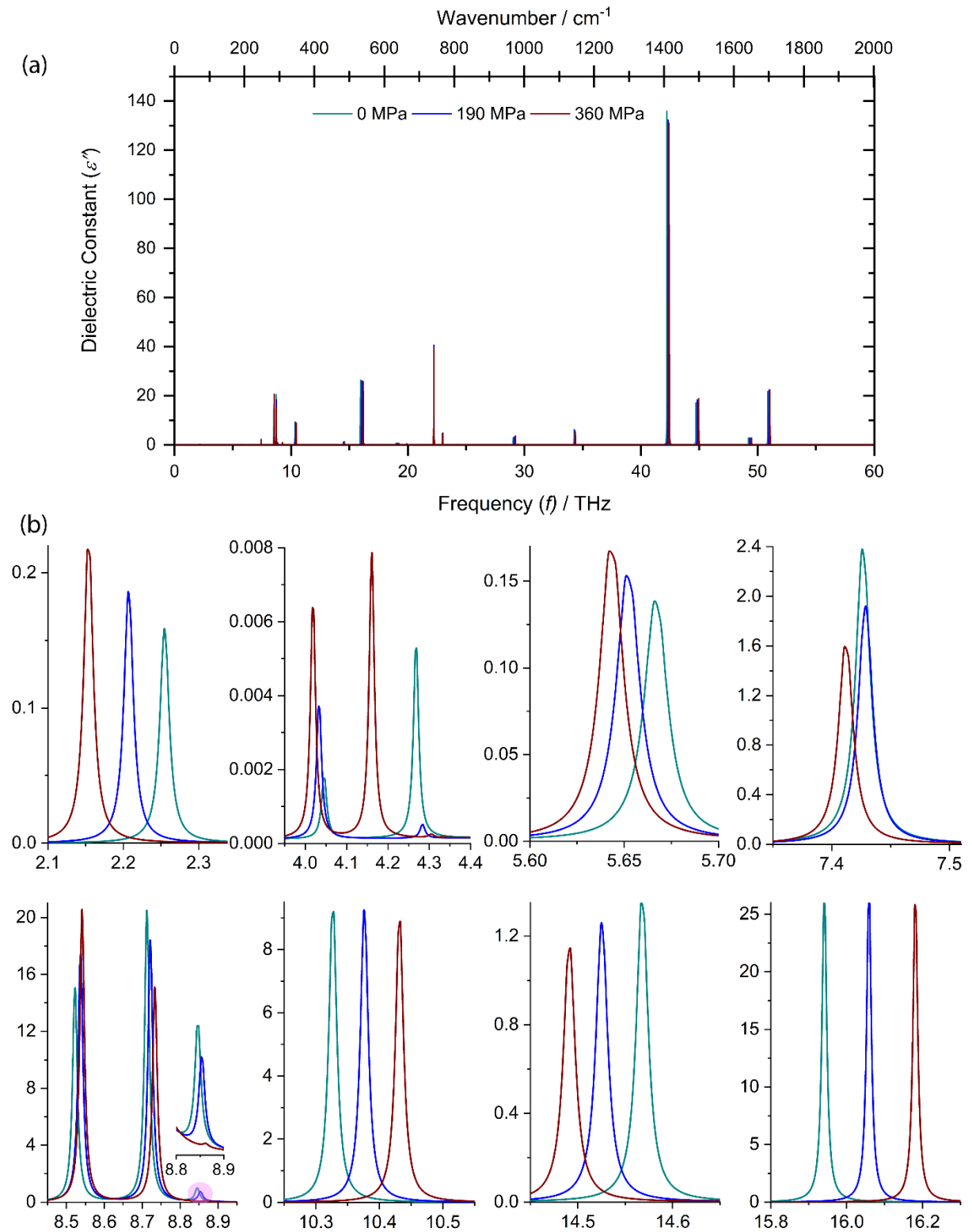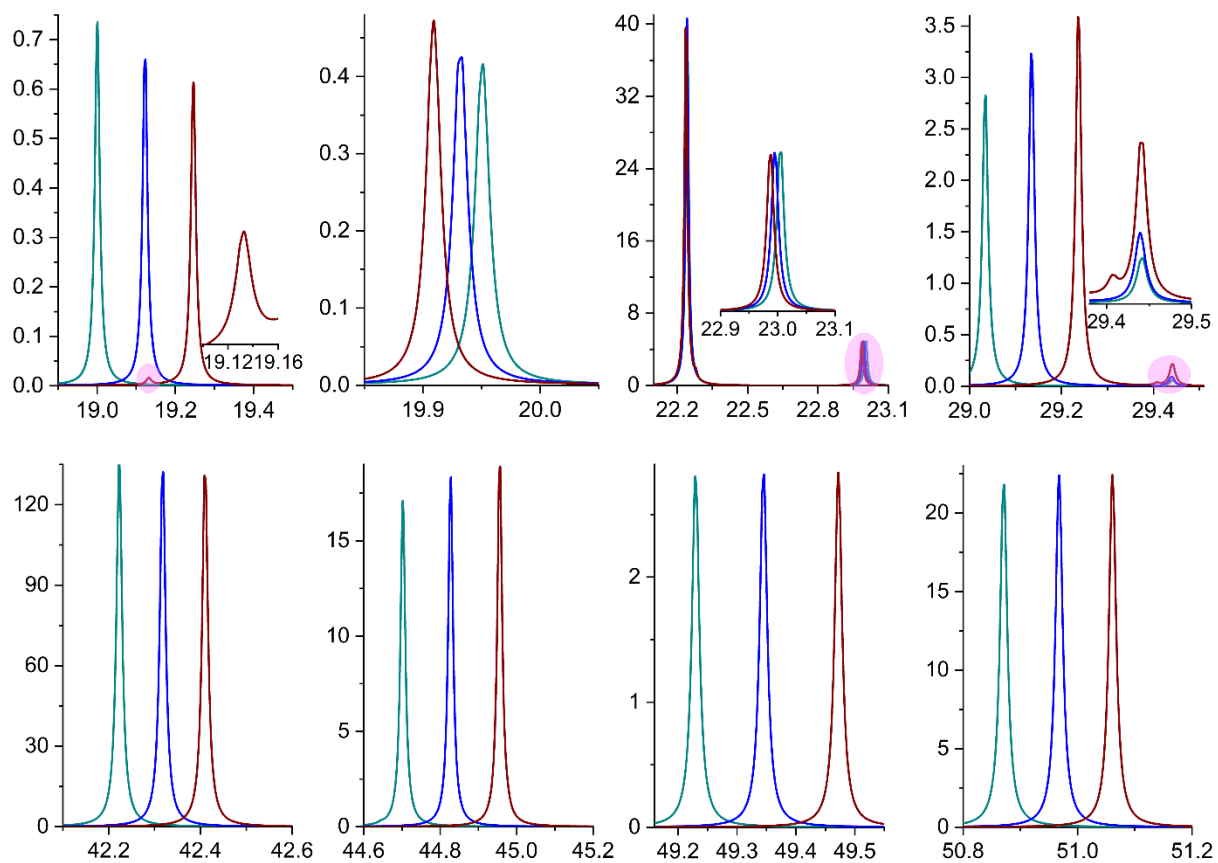
Figure S18: Pressure-dependent dielectric constant calculated by DFT. (a) Imaginary part of the dielectric constant ε''. (b) Zoomed plots of the selected frequencies showing the red/blue shifts.

References

[1]   V. Lucarini, J. J. Saarinen, K. E. Peiponen, E. M. Vartiainen, *Kramers-kronig relations in optical materials research*, Springer-Verlag, Berlin Heidelberg, **2005**.

[2]   K. Titov, Z. Zeng, M. R. Ryder, A. K. Chaudhari, B. Civalleri, C. S. Kelley, M. D. Frogley, G. Cinque, J. C. Tan, *J. Phys. Chem. Lett.* **2017**, *8*, 5035-5040.

[3]   J. M. Chalmers, P. R. Griffiths, *Handbook of vibrational spectroscopy*, Wiley, **2002**.

[4]   M. R. Ryder, T. D. Bennett, C. S. Kelley, M. D. Frogley, G. Cinque, J. C. Tan, *Chem. Commun.* **2017**, *53*, 7041-7044.

[5]   R. Dovesi, A. Erba, R. Orlando, C. M. Zicovich-Wilson, B. Civalleri, L. Maschio, M. Rerat, S. Casassa, J. Baima, S. Salustro, B. Kirtman, *WIREs Comput. Mol. Sci.* **2018**, *8*.

[6]   a) A. D. Becke, *J. Chem. Phys.* **1993**, *98*, 5648-5652; b) C. T. Lee, W. T. Yang, R. G. Parr, *Phys. Rev. B* **1988**, *37*, 785-789.

[7]   S. Grimme, J. Antony, S. Ehrlich, H. Krieg, *J. Chem. Phys.* **2010**, *132*.

[8]   M. F. Peintinger, D. V. Oliveira, T. Bredow, *J. Comput. Chem.* **2013**, *34*, 451-459.

[9]   M. R. Ryder, B. Civalleri, G. Cinque, J. C. Tan, *CrystEngComm* **2016**, *18*, 4303-4312.

[10]   M. De la Pierre, C. Carteret, R. Orlando, R. Dovesi, *J. Comput. Chem.* **2013**, *34*, 1476-1485.